polypeptide type I receptor-deficient mice. J Neurosci 2001;21:5520-7

** **This paper indicates the involvement of PAC1 in psychiatric disease.**

97. Otto C, Martin M, Wolfer DP, et al. Altered emotional behavior in PACAP-type-I-receptor-deficient mice. Brain Res Mol Brain Res 2001;92:78-84

** **This paper indicates the involvement of PAC1 in the psychiatric disease.**

98. Nicot A, Otto T, Brabet P, et al. Altered social behavior in pituitary adenylate cyclase-activating polypeptide type I receptor-deficient mice. J Neurosci 2004;24:8786-95

99. Lang B, Song B, Davidson W, et al. Expression of the human PAC1 receptor leads to dose-dependent hydrocephalus-related abnormalities in mice. J Clin Invest 2006;116(7):1924-34

100. Moser A, Scholz J, Gänsle A. Pituitary adenylate cyclase-activating polypeptide (PACAP-27) enhances tyrosine hydroxylase activity in the nucleus accumbens of the rat., Neuropeptides 1999;33(6):492-7

101. Hong M, Yon L, Fournier A, et al. Effect of pituitary adenylate cyclase-activating polypeptide (PACAP) on tyrosine hydroxylase gene expression in the rat adrenal medulla., Ann N Y Acad Sci 1998;865:478-81

102. Anderson ST, Curlewis JD. PACAP stimulates dopamine neuronal activity in the medial basal hypothalamus and inhibits prolactin. Brain Res 1998;790(1-2):343-6

103. Stella N, Magistretti PJ. Vasoactive intestinal peptide (VIP) and pituitary adenylate cyclase-activating polypeptide (PACAP) potentiate the glutamate-evoked release of arachidonic acid from mouse cortical neurons. Evidence for a cAMP-independent mechanism. J Biol Chem 1996;271(39):23705-10

104. Liu GJ, Madsen BW. PACAP38 modulates activity of NMDA receptors in cultured chick cortical neurons. J Neurophysiol 1997;784:2231-4

105. Pellegri G, Magistretti PJ, Martin JL. VIP and PACAP potentiate the action of glutamate on BDNF expression in mouse cortical neurones. Eur J Neurosci 1998;10(1):272-80

106. Mabuchi T, Shintani N, Matsumura S, et al. Pituitary adenylate cyclase activating polypeptide is required for the development of spinal sensitization and induction of neuropathic pain. J Neurosci 2004;24:7283-91

107. Billingslea EN, Mastropaolo J, Rosse RB, et al. Interaction of stress and strain on glutamatergic neurotransmission: relevance to schizophrenia. Pharmacol Biochem Behav 2003;74(2):351-6

108. Kuroda S, Nakagawa N, Tokunaga C, et al. Mammalian homologue of the Caenorhabditis elegans UNC-76 protein involved in axonal outgrowth is a protein kinase C ζ-interacting protein. J Cell Biol 1999;144:403-11

109. Yamada K, Nakamura K, Minabe Y, et al. Association analysis of FEZ1 variants with schizophrenia in Japanese cohorts. Biol Psychiatry 2004;56:683-90

110. Zhang W, Duan W, Cheung NS, et al. Pituitary adenylate cyclase-activating polypeptide induces translocation of its G-protein-coupled receptor into caveolin-enriched membrane microdomains, leading to enhanced cyclic AMP generation and neurite outgrowth in PC12 cells. J Neurochem 2007;103(3):1157-67

111. Mustafa T, Grimaldi M, Eiden LE. The hop cassette of the PAC1 receptor confers coupling to Ca2+ elevation required for pituitary adenylate cyclase-activating polypeptide-evoked neurosecretion. J Biol Chem 2007;282(11):8079-91

112. Clapcote SJ, Lipina TV, Millar JK, et al. Behavioral phenotypes of Disc1 missense mutations in mice. Neuron 2007;54(3):387-402

* **This paper indicates the involvement of DISC1 in psychiatric disease.**

113. Pickard BS, Thomson PA, Christoforou A, et al. The PDE4B gene confers sex-specific protection against schizophrenia. Psychiatr Genet 2007;17(3):129-33

114. Tardito D, Tura GB, Bocchio L, et al. Abnormal levels of cAMP-dependent protein kinase regulatory subunits in platelets from schizophrenic patients. Neuropsychopharmacology 2000;23(2):216-9

115. Watts VJ. Molecular mechanisms for heterologous sensitization of adenylate cyclase. J Pharmacol Exp Ther 2002;302(1):1-7

116. Okada Y, Miyamoto T, Sato T. Vasopressin increases frog gustatory neural responses elicited by NaCl and HCl. Comp Biochem Physiol A 1991;100(3):693-6

117. Yang X, Horn K, Wand GS., Chronic ethanol exposure impairs phosphorylation of CREB and CRE-binding activity in rat striatum. Alcohol Clin Exp Res 1998;22(2):382-90

118. Nishino N, Kitamura N, Hashimoto T, et al. Increase in [3H]cAMP binding sites and decrease in Giα and Goα immunoreactivities in left temporal cortices from patients with schizophrenia. Brain Res 1993;615(1): 41-9

119. Kerwin RW, Beats BC. Increased forskolin binding in the left parahippocampal gyrus and CA1 region in post mortem schizophrenic brain determined by quantitative autoradiography. Neurosci Lett 1990;118(2):164-8

120. Natsukari N, Kulaga H, Baker I, et al. Increased cyclic AMP response to forskolin in Epstein-Barr virus-transformed human B-lymphocytes derived from schizophrenics. Psychopharmacology (Berl) 1997;130(3):235-41

121. Spaulding SW. The ways in which hormones change cyclic adenosine 3′,5′-monophosphate-dependent protein kinase subunits, and how such changes affect cell behavior. Endocr Rev 1993;14(5):632-50

122. Brandish PE, Su M, Holder DJ, et al. Regulation of gene expression by lithium and depletion of inositol in slices of adult rat cortex. Neuron 2005;45:861-72

** **This paper describes a method to regulate PACAP levels *in vivo*.**

123. Zhu L, Tamvakopoulos C, Xie D, et al. The role of dipeptidyl peptidase IV in the cleavage of glucagon family peptides: in vivo metabolism of pituitary adenylate cyclase activating polypeptide-(1–38). J Biol Chem 2003;278:22418-23

** **This paper describes a method to regulate PACAP levels *in vivo*.**

124. Green BD, Irwin N, Flatt PR. Pituitary adenylate cyclase-activating peptide (PACAP): assessment of dipeptidyl peptidase IV degradation, insulin-releasing activity and antidiabetic potential. Peptides 2006;27(6):1349-58

** **This paper describes a method to regulate PACAP levels *in vivo*.**

125. Kamiya A, Kubo K, Tomoda T, et al. A schizophrenia-associated mutation of DISC1 perturbs cerebral cortex development. Nat Cell Biol 2005;7(12):1167-78

Regulation of pituitary adenylyl cyclase-activating polypeptide (PACAP, ADCYAP1: adenylyl cyclase-activating polypeptide 1) in the treatment of schizophrenia

Affiliation

Shinsuke Matsuzaki[1] & Masaya Tohyama
[1]Author for correspondence
Osaka University,
The Osaka-Hamamatsu Joint Research Center
for Child Mental Development,
Graduate School of Medicine,
Department of Anatomy and Neuroscience,
2-2 Yamadaoka, Suita, Osaka 565-0871, Japan
Tel: +81 6 6879 3221; Fax: +81 6 6879 3229;
E-mail: s-matsuzaki@anat2.med.osaka-u.ac.jp

Biochemical and Biophysical Research Communications 373 (2008) 298–302

Contents lists available at ScienceDirect

Biochemical and Biophysical Research Communications

journal homepage: www.elsevier.com/locate/ybbrc

Behavioral abnormalities and dopamine reductions in *sdy* mutant mice with a deletion in *Dtnbp1*, a susceptibility gene for schizophrenia

Satoko Hattori [a], Tomotaka Murotani [b], Shinsuke Matsuzaki [c,d,e], Tomoko Ishizuka [b,e], Natsuko Kumamoto [c,d,e], Masatoshi Takeda [e,f], Masaya Tohyama [c,d,e], Atsushi Yamatodani [b,e], Hiroshi Kunugi [a], Ryota Hashimoto [*,a,e,f]

[a] Department of Mental Disorder Research, National Institute of Neuroscience, National Center of Neurology and Psychiatry, 4-1-1 Ogawahigashi, Kodaira, Tokyo 187-8502, Japan
[b] Department of Medical Physics and Engineering, Division of Health Sciences, Graduate School of Medicine, Osaka University, 1-7 Yamadaoka, Suita, Osaka 565-0871, Japan
[c] Department of Anatomy and Neuroscience, Graduate School of Medicine, Osaka University, 2-2 Yamadaoka, Suita, Osaka 565-0871, Japan
[d] The 21st Century COE Program, Japan
[e] The Osaka-Hamamatsu Joint Research Center for Child Mental Development, Osaka University Graduate School of Medicine, D3, 2-2 Yamadaoka, Suita, Osaka 565-0871, Japan
[f] Department of Psychiatry, Osaka University Graduate School of Medicine, 2-2 Yamadaoka, Suita, Osaka 565-0871, Japan

ARTICLE INFO

Article history:
Received 6 June 2008
Available online 13 June 2008

Keywords:
Schizophrenia
Dysbindin-1
Locomotor activity
Anxiety
Dopamine
Endophenotype

ABSTRACT

Genetic susceptibility plays an important role in the pathogenesis of schizophrenia. Genetic evidence for an association between the dysbindin-1 gene (*DTNBP1*: dystrobrevin binding protein 1) and schizophrenia has been repeatedly reported in various populations worldwide. Thus, we performed behavioral analyses on homozygous *sandy* (*sdy*) mice, which lack dysbindin-1 owing to a deletion in the *Dtnbp1* gene. Our results showed that *sdy* mice were less active and spent less time in the center of an open field apparatus. Consistent with the latter observation, *sdy* mice also displayed evidence of heightened anxiety-like response and deficits in social interaction. Compared to wild-type mice, *sdy* mice displayed lower levels of dopamine, but not glutamate, in the cerebral cortex, hippocampus, and hypothalamus. These findings indicate that *sdy* mice display a number of behavioral abnormalities associated with schizophrenia and suggest that these abnormalities may be mediated by reductions in forebrain dopamine transmission.

Schizophrenia is characterized by psychosis and profound disturbances of cognition, emotion, and social functioning. The dysbindin-1 gene (*DTNBP1*: dystrobrevin binding protein 1), have recently been identified as a susceptibility gene for schizophrenia [1,2]. In studies on postmortem brain tissue, decreased expression levels of dysbindin-1 protein [3] and mRNA [4] have been shown in patients with schizophrenia compared with controls. Chronic treatment of mice with antipsychotics did not affect the expression levels of dysbindin-1 protein and mRNA in their brains [3,5], suggesting that prior evidence of lower levels of dysbindin-1 protein and mRNA in the postmortem brains of schizophrenics is not likely to be a simple artifact of antemortem drug treatment. These data indicate that the dysbindin-1 gene may confer susceptibility to schizophrenia through reduced expression.

Dysbindin-1 is relatively ubiquitously expressed in neuronal cell bodies in most parts of the brain and in primary dendrites of those neurons and is concentrated in axon terminals of some areas such as the hippocampal formation, striatum, substantia nigra, and cerebellum [3,6]. Previous studies reported that down-regulation of endogenous dysbindin-1 by small interfering RNA (siRNA) resulted in a reduction in the release of glutamate from primary cultured neurons [7] and an increase in the release of dopamine from PC12 cells [8]. These results suggest possible roles for the dysbindin-1 gene in glutamatergic and dopaminergic systems related to the pathophysiology of schizophrenia [9].

To investigate the functions of dysbindin-1 *in vivo*, we analyzed *sandy* (*sdy*) mutant mice, which express no dysbindin-1 protein owing to a deletion in the dysbindin-1 gene [10]. *Sdy* is a mutant mouse with diluted pigmentation that arose spontaneously in the DBA/2J inbred mouse strain and has simultaneous defects in melanosomes, lysosomes and platelet dense granules [11]. Thus, we first performed several behavioral analyses and measured dopamine and glutamate contents in several brain regions in *sdy* mice.

Materials and methods

Animals. We obtained *sdy* mice from the Jackson Laboratory (Bar Harbor, ME). *Sdy* mice have an autosomal recessive coat color

* Corresponding author. Address: The Osaka-Hamamatsu Joint Research Center for Child Mental Development, Osaka University Graduate School of Medicine, D3, 2-2 Yamadaoka, Suita, Osaka 565-0871, Japan. Fax: +81 6 6879 3059.
E-mail address: hashimor@psy.med.osaka-u.ac.jp (R. Hashimoto).

0006-291X/$ - see front matter © 2008 Elsevier Inc. All rights reserved.
doi:10.1016/j.bbrc.2008.06.016

mutation that arose spontaneously in the inbred DBA/2J strain. *Sdy* mice have a large deletion in the dysbindin-1 gene, from nucleotide 3701 of intron 5 to nucleotide 12377 of intron 7, and this deletion results in essentially total loss of dysbindin-1 [10]. Both *sdy* mice and wild-type mice derived from heterozygote crossings were used in all experiments. To minimize the influence of cage environment, they were bred under the same conditions after weaning at 3 weeks of age. The genotypes of mice were identified by their coat color and genomic PCR. Primers i6_f (5′-GCACTCAGGA GACCATGACA-3′) and i6_r (5′-GGTTGACACTCTTGCGGAAT-3′) amplified a region in intron 6, and produced 305 bp PCR products from normal DNA. Primers i5, designed for intron 5 (5′-CCTAGCCCC TCAGGAATTGT-3′), and i7, designed for intron 7 (5′-GGGAATGGG GTCTTAATGGT-3′), amplified 733 bp PCR products from mutant DNA. The genomic sequences of these PCR products were confirmed by sequence analysis. The experimental protocols were approved by the Ethics Review Committee for Animal Experimentation of the National Institute of Neuroscience, Japan.

Experimental design for behavioral tests. All behavioral tests were carried out as described previously [12] using male mice that were 6–9 weeks old (*sdy* mice: $n = 119$; wild-type mice: $n = 120$). We used different batches of mice for each behavioral test. Mice were housed four per cage in a temperature-controlled room under a 12 h light–dark cycle (light on at 8:00 a.m.) with ad libitum access to food and water. All behavioral tests were performed between 10:00 a.m. and 7:00 p.m. After each trial, all apparatus were cleaned with water to prevent a bias based on olfactory cues.

Open field test. Locomotor activity was measured using an open field test. Activity was recorded during the first exposure to the open field apparatus (50 × 50 × 40 cm; O'Hara & Co., Tokyo, Japan). The illumination level was 40 lux at the floor of the open field. The field was divided by software (see below) into 16 equal-sized squares containing 4 central areas and 12 peripheral areas. Time spent in the central area defined as [stay time in center (%) = time spent in central areas/objective time for analysis (15 min or 30 min)] and the number of fecal boli were recorded. Data were collected for 30 min. Data acquisition and analysis were performed automatically, using Image OF software (see Behavioral data analysis).

Elevated plus maze test. The elevated plus maze consisted of two black plastic walkways (25 × 5 cm) 34 cm above the floor intersecting at right angles with one of the walkways having 15 cm high wall. To prevent animals from falling off the apparatus, 3-mm-high ledges were provided on the open arms (O'Hara & Co., Tokyo, Japan). A mouse was placed in the central square of the maze (5 × 5 cm), facing one of the enclosed arms. The behavior was recorded during a 20 min test session, because mice entered into the open arms a few times (*sdy* mice; 2.1 ± 0.7, wild-type mice; 3.6 ± 0.8) for a 10 min test session. The illumination level was 40 lux at the central square of the maze. For data analysis, we used the following four measures: the number of entries into open arms, the total number of arm entries, the time spent on the open arms and the total distance traveled. Data acquisition and analysis were performed automatically, using Image EP software (see Behavioral data analysis).

Social interaction test. A pair of mice was placed simultaneously at opposing corners in the open field apparatus (50 × 50 × 40 cm; O'Hara & Co., Tokyo, Japan) and allowed to explore freely for 30 min. The pair of mice tested was composed of the same genotype (*sdy*–*sdy* pair or wild–wild pair) and had been housed in the same environmental conditions, but in different cages. The illumination level was 40 lux at the floor of the open field. Mice were familiar with the test arena by placing them singly in the apparatus, under the same light level (40 lux), for a 30 min period at least 2 days preceding the test. Total duration of contacts, the number of contacts and total distance traveled were measured. Analysis was performed automatically using Image SI software (see Behavioral data analysis).

Behavioral data analysis. Behavioral data from the open field tests, elevated plus maze tests and social interaction tests were automatically analyzed as described previously [12]. Briefly, behaviors were monitored by a color charged-coupled device camera (Watec Co., Ltd., Yamagata, Japan) that was connected to a Macintosh computer. We used apparatuses with black-colored floors to detect behaviors of mice, because coat colors of mice were whitish (*sdy*) and dilute brown (wild-type). Images were captured at one or two frames per second. The applications used for the behavioral studies (Image OF, Image EP, Image SI, O'Hara & Co., Tokyo, Japan) were run using a Macintosh computer. These modified applications were based on the public domain NIH Image program developed at the U.S. National Institute of Mental Health.

Neurotransmitter measurements by HPLC-fluorometry. We measured the dopamine and glutamate levels in intact brain with a different batch of mice used for behavioral tests. Mice (male: 8–12 weeks old) were sacrificed by decapitation, and the decapitated heads were dropped directly into ice-cold water for 1 s to prevent degradation of neurotransmitters. Brains were removed from the calvarium and put on a chilled aluminum board. The brain was dissected into ten regions (olfactory bulb, OB; frontal pole cortex, FPC; non-frontal cerebral cortex, NF CX; cerebellum, CB; hippocampal formation, HF; striatum, ST; midbrain, MB; lower brainstem, LB; thalamus, TH; hypothalamus, HT) according to a previously reported method [13] with slight modification. Each block of brain tissue was put into a pre-weighed sampling tube. Brain tissues were homogenized in 9 volumes of 2% perchloric acid (PCA) solution (Katayama Chemical Industries Co., Ltd., Japan) including 1 mM EDTA-Na_2 and 1 mM $Na_2S_2O_5$ using a sonicator for 5–10 s. Homogenates were centrifuged at 10,000*g* for 30 min. The level of dopamine in the supernatant was determined by a fully automated HPLC system (Model HLC-725CA Catecholamine analyzer, Tosoh, Tokyo, Japan) using a diphenylethylenediamine condensation method [14]; glutamate levels were measured by a pre-label HPLC-fluorometric method [15].

Statistical analysis. Statistical analysis was conducted using SPSS 11.0J for Windows (SPSS Japan Inc., Tokyo, Japan). Data were analyzed by a two-tailed *t*-test unless otherwise noted. Fisher's exact test was used to compare *sdy* mice with wild-type mice for general health (physical characteristics, sensory/motor reflexes and the motor test). A repeated measures analysis of variance (ANOVA) was used to analyze differences in the time course of distance traveled in the open field test. For measurements of neurotransmitters, statistical significance was analyzed using the Student's *t*-test. All *p*-values reported are two-tailed. Statistical significance was defined as $p < 0.05$.

Results

General characteristics

There was no significant difference in body weight, physical characteristics (whiskers and fur), sensory-motor reflexes (eye blink, ear twitch, whisker response and righting reflex) or neuromuscular strength between *sdy* mice and wild-type mice (Supplementary Table S1). *Sdy* mice were more sensitive to 120DB auditory stimulation than wild-type mice, however, there was no significant difference in PPI between *sdy* and wild-type mice (data not shown).

Locomotor activity in a novel environment

Sdy mice showed a pronounced decrease in locomotor activity in the open field test compared with wild-type mice (Fig. 1A, geno-

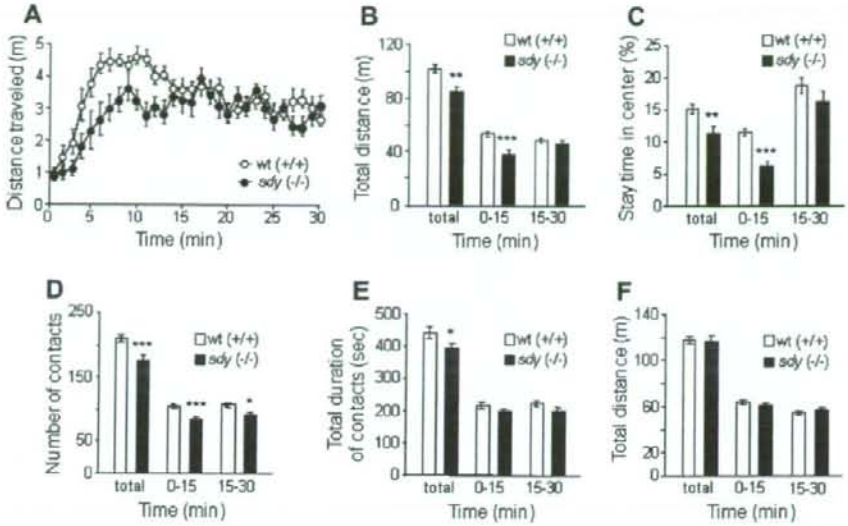

Fig. 1. Open field test with *sdy* mice (A–C). Time course of distance traveled (A), total distance traveled (B) and time spent in the central area (C), are shown (*sdy* mice: $n = 18$, wild-type mice: $n = 21$). Social interaction test in *sdy* mice (D–F). The total number of contacts (D), total duration of contacts (E) and distance traveled (F), in the social interaction test, are shown (pairs of *sdy* mice: $n = 22$, pairs of wild-type mice: $n = 21$). Data represent means ± SEM. $^{*}p < 0.05$, $^{**}p < 0.01$, $^{***}p < 0.001$, compared with wild-type mice.

type effect, $F(1,37) = 12.3$, $p = 0.001$). This hypoactivity phenotype was notable during the first half of the test period (Fig. 1B, total: $t(37) = 3.51$, $p = 0.001$, 0–15 min: $t(37) = 3.82$, $p < 0.001$, 15–30 min: $t(37) = 0.68$, $p = 0.50$). We then compared time spent in the center of the open field apparatus between *sdy* and wild-type mice. As shown in Fig. 1C, *sdy* mice spent significantly less time in the center (total: $t(37) = 2.99$, $p = 0.005$, 0–15 min: $t(37) = 5.26$, $p < 0.001$, 15–30 min: $t(37) = 1.19$, $p = 0.24$). There was no significant difference in the number of fecal boli during the open field test between *sdy* and wild-type mice (*sdy* mice: 8.0 ± 0.6, wild-type mice: 9.3 ± 1.0, $t(37) = 1.15$, $p = 0.26$).

Social interaction test

In the social interaction test, *sdy* mice showed a significant decrease in the number of social contacts compared with wild-type mice (Fig. 1D, total: $t(41) = 3.57$, $p < 0.001$, 0–15 min: $t(41) = 3.87$, $p < 0.001$, 15–30 min: $t(41) = 2.65$, $p = 0.012$). The total duration of contacts was also decreased in *sdy* mice during a 30 min test session (Fig. 1E, total: $t(41) = 2.05$, $p = 0.047$, 0–15 min: $t(41) = 1.49$, $p = 0.14$, 15–30 min: $t(41) = 1.71$, $p = 0.095$). The total distance traveled was not significantly different between the two genotypes (Fig. 1F, total: $t(41) = 0.24$, $p = 0.81$, 0–15 min: $t(41) = 1.01$, $p = 0.32$, 15–30 min: $t(41) = 0.62$, $p = 0.54$).

Elevated plus maze test

In the elevated plus maze test, *sdy* mice exhibited a trend toward a reduced number of entries into the open arms during a 20 min test session compared with wild-type mice (Fig. 2A, total: $t(32) = 2.00$, $p = 0.054$). During the second half of the test period, the number of entries into the open arms was significantly lower in *sdy* mice than wild-type mice (Fig. 2A), 0–10 min: $t(32) = 1.41$, $p = 0.17$, 10–20 min: $t(32) = 2.11$, $p = 0.042$). *Sdy* mice also showed a significant decrease in the total number of arm entries during the second half of the test period and across the entire test period compared with wild-type mice (Fig. 2B, total: $t(32) = 2.35$, $p = 0.025$, 0–10 min: $t(32) = 2.00$, $p = 0.054$, 10–20 min: $t(32) = 2.19$, $p = 0.036$).

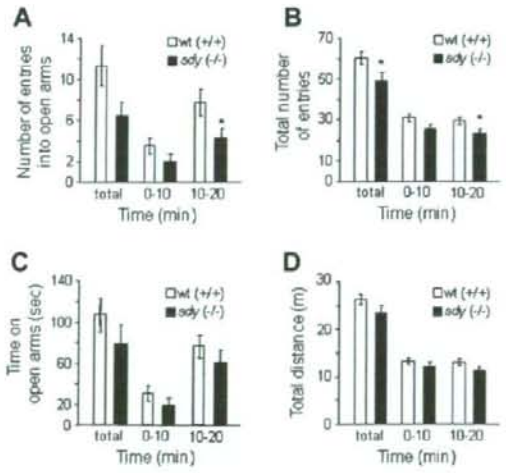

Fig. 2. Elevated plus maze test in *sdy* mice. The number of open arm entries (A), total number of arm entries (B), time on open arms (C), and distance traveled (D), are shown (*sdy* mice: $n = 16$, wild-type mice: $n = 18$). Data represent means ± SEM. $^{*}p < 0.05$, compared with wild-type mice.

There were no significant differences in the amount of time spent on the open arms (Fig. 2C, total: $t(32) = 1.13$, $p = 0.27$, 0–10 min: $t(32) = 1.18$, $p = 0.25$, 10–20 min: $t(32) = 0.94$, $p = 0.35$) or in the total distance traveled (Fig. 2D, total: $t(32) = 1.56$, $p = 0.13$, 0–10 min: $t(32) = 1.09$, $p = 0.28$, 10–20 min: $t(32) = 1.69$, $p = 0.10$) between *sdy* mice and wild-type mice.

Dopamine and glutamate contents in the brain

Dopamine content was significantly reduced in three brain regions of *sdy* mice compared with wild-type mice: non-frontal cerebral cortex (*sdy* mice: 0.114 nmol/g, wild-type mice: 0.222 nmol/g,

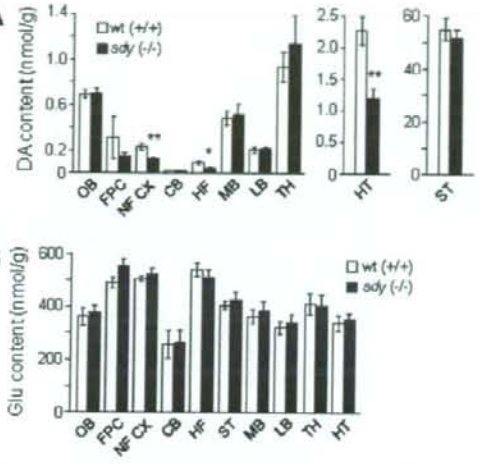

Fig. 3. Dopamine and glutamate content in the brains of *sdy* mice. Dopamine (DA) content (A) and glutamate (Glu) content (B) are shown (dopamine: $n = 4$–8, glutamate: $n = 11$). Olfactory bulb, OB; frontal pole cortex, FPC; non-frontal cerebral cortex, NF CX; cerebellum, CB; hippocampal formation, HF; striatum, ST; midbrain, MB; lower brainstem, LB; thalamus, TH; hypothalamus, HT. Data represent means ± SEM. $^{*}p < 0.05$, $^{**}p < 0.01$ compared with wild-type mice.

$p = 0.002$), hippocampal formation (*sdy* mice: 0.0392 nmol/g, wild-type mice: 0.0822 nmol/g, $p = 0.03$), and hypothalamus (*sdy* mice: 1.17 nmol/g, wild-type mice: 2.26 nmol/g, $p = 0.007$) (Fig. 3A). However, no significant difference in glutamate content was detected between *sdy* and wild-type mice in the brain areas examined (Fig. 3B).

Discussion

Several schizophrenia-related behaviors in rodents, such as hyperactivity, deficits in PPI, locomotor response to antipsychotics, disturbance in social interactions, and cognitive deficits, have commonly been observed in previous animal models for schizophrenia [16]. We report here that *sdy* mice, which express no dysbindin-1, show some, but not all, of these abnormalities.

In the open field test, *sdy* mice exhibited decreased locomotor activity during the first half of the test period compared with wild-type mice, and did not show habituation in a novel environment (Fig. 1A and B). It is unlikely that these abnormalities are due to a loss of motor function or general activity, which could be detected by the open field test, because of no differences in locomotor activity during the second half of the test or in neuromuscular strength between the two groups of animals. It could be caused by reduced adaptation, motivation to explore, and/or enhanced anxiety-like response in a novel environment. Indeed, *sdy* mice spent significantly less time in the center of the open field apparatus than wild-type mice (Fig. 1C), which is associated with anxiety-like response [17]. In addition, *sdy* mice showed a decrease in the number of entries into open arms and in the total number of arm entries in the elevated plus maze test (Fig. 2A and B), suggesting enhanced anxiety-related behavior in *sdy* mice. In the social interaction test, *sdy* mice showed reductions in the number of contacts and in the total duration of contacts without hypoactivity (Fig. 1D–F). The decreased social interactions may be caused largely by the proposed anxiogenic-like phenotype of the *sdy* mice and possibly by the reduced exploration. In rodents, reduced contacts with unfamiliar partners are indicative of social withdrawal, a clinical aspect of schizophrenia [16], suggesting a social withdrawal phenotype in *sdy* mice. Previous study demonstrated that retinal melanosomes were deficient in *sdy* mice [10]. As we did not examine the visual acuity in *sdy* mice, there is a possibility that reduced visual acuity resulting from retinal defects affects multiple behavioral parameters in this study. Increased locomotor activity, which is observed in most animal models of schizophrenia, is considered to be a positive symptom of schizophrenia, like delusions and hallucinations. However, *sdy* mice showed less activity, which is unique in an animal model for schizophrenia. This phenotype could be due to a decreased motivation to explore, which might be related to the negative symptoms of schizophrenia (blunted affect, decreased motivation, and social withdrawal). Other phenotypes such as less time in the center of the open field apparatus, abnormal response in elevated plus maze, and decreased social interactions could also be related to reduced exploratory tendencies. Indeed, two recent studies show a significant association between risk haplotypes of the dysbindin-1 gene and negative symptoms in patients with schizophrenia [18,19]. These data imply that *sdy* mice, which exhibit reduced exploratory activity, heightened anxiety-like response and deficits in social interaction, could be a potential genetic model for negative symptom endophenotypes of schizophrenia.

Decreased dopamine content in three brain regions of *sdy* mice measured by HPLC-fluorometry in the present study (Fig. 3A) was consistent with dopamine reduction measured by HPLC with an electrochemical detection in the previous study [20]. Recent studies reported that reduced dysbindin-1 protein by *DTNBP1* siRNA transfection increased surface expression of dopamine D2 receptor (DRD2) and blocked dopamine-induced internalization of DRD2 in SH-SY5Y cells [21], and that dopamine release was increased by siRNA-mediated silencing of dysbindin-1 protein in PC12 cells [8]. These results suggest that the lack of dysbindin-1 causes an imbalance of the dopaminergic system. As DRD2 mutant mice show decreased activity [22,23], decreased locomotor activity in *sdy* mice could be due to the abnormal regulation of dopaminergic system by lack of dysbindin-1 protein. As glutamate content in *sdy* mouse brain was not altered, behavioral abnormalities in *sdy* mice could be related to the dopaminergic system rather than the glutamatergic system.

This new genetic mouse model could shed light on the etiology of schizophrenia and lead us to new hypotheses, novel diagnostic tools, and more effective therapies for the disorder.

Acknowledgments

This work was supported in part by the Japanese Ministry of Education, Culture, Sports, Science and Technology, CREST of JST, and Grant-in-Aid for Scientific Research on Priority Areas -Research on Pathomechanisms of Brain Disorders- from the MEXT (18023045).

Appendix A. Supplementary data

Supplementary data associated with this article can be found, in the online version, at doi:10.1016/j.bbrc.2008.06.016.

References

[1] P.J. Harrison, D.R. Weinberger, Schizophrenia genes, gene expression, and neuropathology: on the matter of their convergence, Mol. Psychiatry 10 (2005) 40–68.

[2] R. Hashimoto, S. Hattori, S. Chiba, Y. Yagasaki, T. Okada, E. Kumamaru, T. Mori, K. Nemoto, H. Tanii, H. Hori, H. Noguchi, T. Numakawa, T. Ohnishi, H. Kunugi, Susceptibility genes for schizophrenia, Psychiatry Clin. Neurosci. 60 (Suppl 1) (2006) S4–S10.

[3] K. Talbot, W.L. Eidem, C.L. Tinsley, M.A. Benson, E.W. Thompson, R.J. Smith, C.G. Hahn, S.J. Siegel, J.Q. Trojanowski, R.E. Gur, D.J. Blake, S.E. Arnold, Dysbindin-1

is reduced in intrinsic, glutamatergic terminals of the hippocampal formation in schizophrenia, J. Clin. Invest. 113 (2004) 1353–1363.
[4] C.S. Weickert, R.E. Straub, B.W. McClintock, M. Matsumoto, R. Hashimoto, T.M. Hyde, M.M. Herman, D.R. Weinberger, J.E. Kleinman, Human dysbindin (DTNBP1) gene expression in normal brain and in schizophrenic prefrontal cortex and midbrain, Arch. Gen. Psychiatry 61 (2004) 544–555.
[5] S. Chiba, R. Hashimoto, S. Hattori, M. Yohda, B. Lipska, D.R. Weinberger, H. Kunugi, Effect of antipsychotic drugs on DISC1 and dysbindin expression in mouse frontal cortex and hippocampus, J. Neural. Transm. 113 (2006) 1337–1346.
[6] K. Talbot, D.S. Cho, W.Y. Ong, M.A. Benson, L.Y. Han, H.A. Kazi, J. Kamins, C.G. Hahn, D.J. Blake, S.E. Arnold, Dysbindin-1 is a synaptic and microtubular protein that binds brain snapin, Hum. Mol. Genet. 15 (2006) 3041–3054.
[7] T. Numakawa, Y. Yagasaki, T. Ishimoto, T. Okada, T. Suzuki, N. Iwata, N. Ozaki, T. Taguchi, M. Tatsumi, K. Kamijima, R.E. Straub, D.R. Weinberger, H. Kunugi, R. Hashimoto, Evidence of novel neuronal functions of dysbindin, a susceptibility gene for schizophrenia, Hum. Mol. Genet. 13 (2004) 2699–2708.
[8] N. Kumamoto, S. Matsuzaki, K. Inoue, T. Hattori, S. Shimizu, R. Hashimoto, A. Yamatodani, T. Katayama, M. Tohyama, Hyperactivation of midbrain dopaminergic system in schizophrenia could be attributed to the down-regulation of dysbindin, Biochem. Biophys. Res. Commun. 345 (2006) 904–909.
[9] J.M. Stone, P. Morrison, L.S. Pilowsky, Glutamate and dopamine dysregulation in schizophrenia – a synthesis and selective review, J. Psychopharmacol. 21 (2007) 440–452.
[10] W. Li, Q. Zhang, N. Oiso, E.K. Novak, R. Gautam, E.P. O'Brien, C.L. Tinsley, D.J. Blake, R.A. Spritz, N.G. Copeland, N.A. Jenkins, D. Amato, B.A. Roe, M. Starcevic, E.C. Dell'Angelica, R.W. Elliott, V. Mishra, S.F. Kingsmore, R.E. Paylor, R.T. Swank, Hermansky–Pudlak syndrome type 7 (HPS-7) results from mutant dysbindin, a member of the biogenesis of lysosome-related organelles complex 1 (BLOC-1), Nat. Genet. 35 (2003) 84–89.
[11] R.T. Swank, H.O. Sweet, M.T. Davisson, M. Reddington, E.K. Novak, Sandy: a new mouse model for platelet storage pool deficiency, Genet. Res. 58 (1991) 51–62.
[12] S. Hattori, R. Hashimoto, T. Miyakawa, H. Yamanaka, H. Maeno, K. Wada, H. Kunugi, Enriched environments influence depression-related behavior in adult mice and the survival of newborn cells in their hippocampi, Behav. Brain Res. 180 (2007) 69–76.
[13] J. Glowinski, L.L. Iversen, Regional studies of catecholamines in the rat brain. I. The disposition of [3H]norepinephrine, [3H]dopamine and [3H]dopa in various regions of the brain, J. Neurochem. 13 (1966) 655–669.
[14] H. Nohta, A. Mitsui, Y. Ohkura, Spectrofluorometric determination of catecholamines with 1,2-diphenylethylenediamine, Anal. Chim. Acta 165 (1984) 171–176.
[15] H. Tamura, T.P. Hicks, Y. Hata, T. Tsumoto, A. Yamatodani, Release of glutamate and aspartate from the visual cortex of the cat following activation of afferent pathways, Exp. Brain Res. 80 (1990) 447–455.
[16] B.K. Lipska, D.R. Weinberger, To model a psychiatric disorder in animals: schizophrenia as a reality test, Neuropsychopharmacology 23 (2000) 223–239.
[17] J.N. Crawley, What's Wrong with My Mouse? Wiley-Liss, New York, 2000.
[18] A.H. Fanous, E.J. van den Oord, B.P. Riley, S.H. Aggen, M.C. Neale, F.A. O'Neill, D. Walsh, K.S. Kendler, Relationship between a high-risk haplotype in the DTNBP1 (dysbindin) gene and clinical features of schizophrenia, Am. J. Psychiatry 162 (2005) 1824–1832.
[19] P. DeRosse, B. Funke, K.E. Burdick, T. Lencz, J.M. Ekholm, J.M. Kane, R. Kucherlapati, A.K. Malhotra, Dysbindin genotype and negative symptoms in schizophrenia, Am. J. Psychiatry 163 (2006) 532–534.
[20] T. Murotani, T. Ishizuka, S. Hattori, R. Hashimoto, S. Matsuzaki, A. Yamatodani, High dopamine turnover in the brains of Sandy mice, Neurosci. Lett. 421 (2007) 47–51.
[21] Y. Iizuka, Y. Sei, D.R. Weinberger, R.E. Straub, Evidence that the BLOC-1 protein dysbindin modulates dopamine D2 receptor internalization and signaling but not D1 internalization, J. Neurosci. 27 (2007) 12390–12395.
[22] J.H. Baik, R. Picetti, A. Saiardi, G. Thiriet, A. Dierich, A. Depaulis, M. Le Meur, E. Borrelli, Parkinsonian-like locomotor impairment in mice lacking dopamine D2 receptors, Nature 377 (1995) 424–428.
[23] M.A. Kelly, M. Rubinstein, T.J. Phillips, C.N. Lessov, S. Burkhart-Kasch, G. Zhang, J.R. Bunzow, Y. Fang, G.A. Gerhardt, D.K. Grandy, M.J. Low, Locomotor activity in D2 dopamine receptor-deficient mice is determined by gene dosage, genetic background, and developmental adaptations, J. Neurosci. 18 (1998) 3470–3479.

Induction of Amyloid β Accumulation by ER Calcium Disruption and Resultant Upregulation of Angiogenic Factors in ARPE19 Cells

Yoshihisa Koyama,[1,2] Shinsuke Matsuzaki,[1,2,3] Fumi Gomi,[4] Kohei Yamada,[1,2] Taiichi Katayama,[5] Kohji Sato,[5] Tatsuro Kumada,[6] Atsuo Fukuda,[6] Satoshi Matsuda,[4] Yasuo Tano,[4] and Masaya Tohyama[1,2,3]

Purpose. To investigate the intracellular mechanisms that induce amyloid β (Aβ) accumulation and angiogenesis in the human retinal pigment epithelial cell line ARPE19.

Methods. The authors used two endoplasmic reticulum (ER) stress-inducing reagents, thapsigargin (TG), which inhibits the sarcoplasmic/endoplasmic calcium $(Ca)^{2+}$-ATPase, and tunicamycin (TM), which inhibits N-linked glycosylation. The expression pattern of Aβ-precursor protein (APP) splice variants was investigated by reverse transcription (RT)-PCR. Cellular expressions of both a series of Aβ metabolism-related factors and angiogenic factors were evaluated by real-time RT-PCR and Western blot (VEGF). Expression of caspase-4 was examined by real-time RT-PCR and Western blot to evaluate the effect of the ER stressor. Intracellular Ca elevation by TG was evaluated by Ca^{2+} imaging experiments. Dimethyl sulfoxide and staurosporine were used as a nonreagent control and as an apoptosis-inducing reagent through mitochondria not ER, respectively.

Results. TG-treated ARPE19 cells increased the mRNA expression of Aβ production-inducing *APP* splice variants and reduced that of neprilysin, a catabolic enzyme for Aβ. TG-treated ARPE19 cells produced increases in *VEGF*, *TNF-α*, *TACE* mRNA, and VEGF protein expressions and a decrease in *PEDF* mRNA expression. TG-treated ARPE19 cells induced the expression of active more than TM-treated casepase-4. The intracellular Ca concentration was elevated in only TG-treated ARPE19 cells.

Conclusions. TG-treated ARPE19 cells showed both Aβ accumulation-inducible and angiogenic factor mRNA expression patterns. This study suggests the possibility that ER stress through ER calcium disruption may induce the expression not only of Aβ deposit-promoting factors but also angiogenic factors in the retinal pigment epithelium. (*Invest Ophthalmol Vis Sci.* 2008;49:2376–2383) DOI:10.1167/iovs.07-1067

From the Departments of [1]Anatomy and Neuroscience and [4]Ophthalmology, and the [5]Osaka-Hamamatsu Joint Research Center for Child Mental Development, Graduate School of Medicine, Osaka University, Suita, Osaka, Japan; the [2]21st Century COE Program; and the Departments of [3]Anatomy and Neuroscience and [6]Physiology, Hamamatsu University School of Medicine, Shizuoka, Japan.

Submitted for publication August 15, 2007; revised December 26, 2007; accepted April 11, 2008.

Disclosure: **Y. Koyama**, None; **S. Matsuzaki**, None; **F. Gomi**, None; **K. Yamada**, None; **T. Katayama**, None; **K. Sato**, None; **T. Kumada**, None; **A. Fukuda**, None; **S. Matsuda**, None; **Y. Tano**, None; **M. Tohyama**, None

The publication costs of this article were defrayed in part by page charge payment. This article must therefore be marked "*advertisement*" in accordance with 18 U.S.C. §1734 solely to indicate this fact.

Corresponding author: Shinsuke Matsuzaki, Department of Anatomy and Neuroscience, Graduate School of Medicine, Osaka University, 2-2 Yamadaoka, Suita, Osaka 565-0871, Japan; s-matsuzaki@anat2.med.osaka-u.ac.jp.

Age-related macular degeneration (AMD) is the most common cause of irreversible vision loss in the elderly.[1] Although our understanding of molecular events presaging AMD has grown in the past decade, the pathogenesis of AMD remains poorly understood. AMD is classified as dry or nonexudative AMD and as wet or exudative AMD. The most severe complication in wet or exudative AMD is the development of choroidal neovascularization (CNV), which originates in choroidal blood vessels that grow through Bruch membrane into the sub-retinal pigment epithelium (RPE) or the subretinal space, or both. The clinical hallmark of AMD is the appearance of drusen,[2] localized deposits lying between the basement membrane of the RPE and Bruch membrane.

Recently, new evidence has indicated that, in AMD, substructural elements within drusen contain amyloid β (Aβ),[3–5] which is a major component of senile plaques and cerebrovascular deposits found in the brains of patients with Alzheimer disease (AD). Aβ accumulation has been reported to increase the expression of an angiogenic growth factor, vascular endothelial growth factor (VEGF), which plays an important role in conditions that involve ocular angiogenesis, including CNV,[6–9] and to decrease the expression of the potent antiangiogenic factor[10,11] pigment epithelium-derived factor (PEDF), secreted by retinal pigment epithelial cells.[12] These results suggest that Aβ is related to the pathogenesis of AMD. However, the mechanisms that induce the accumulation of Aβ in the RPE of AMD patients have not been determined.

Aβ is known to be a physiological peptide, the steady state level of which is maintained by a metabolic balance between synthesis and degradation, and is constitutively secreted from cells.[13,14] In the amyloidogenic pathway, Aβ is produced by the sequential proteolytic processing of Aβ-precursor protein (APP) by the β site APP cleaving enzyme (BACE) and a presenilin complex.[15–17] Under physiological conditions, Aβ is degraded by peptidases, such as neprilysin[18] and endothelin-converting enzyme (ECE),[19] immediately after production.[20]

Endoplasmic reticulum (ER) stress, which leads to the accumulation of unfolded protein, results in ER dysfunction and subsequent cell death.[21] Neuro 2a cells expressing presenilin2-splice variants, which is expressed in human brains in sporadic AD, or the dominant-negative form of Ire1 are vulnerable to ER stress and to increased Aβ production.[22] Therefore, ER stress plays an important role in Aβ accumulation. We used two ER-stress inducers, thapsigargin (TG) and tunicamycin (TM), in this study. TG, a highly lipophilic sesquiterpene lactone, is broadly used as a selective inhibitor of the sarcoplasmic reticulum calcium-ATPase, which pumps Ca^{2+} from the cytosol into the lumen of ER in mammalian cells. TG-mediated irreversible inhibition of ER Ca^{2+} ATPases can also cause the induction of Ca^{2+} leakage from the ER to the cytoplasm, further facilitating the depletion of Ca^{2+} within the ER, and can result in increases in cytoplasmic Ca^{2+} levels.[23] Long-term elevations of intracellular Ca induced ER stress from abnormal accumulations of folding protein.[24,25] TM is the glucosamine-containing

Investigative Ophthalmology & Visual Science, June 2008, Vol. 49, No. 6

nucleoside antibiotic generated by *Streptomyces* and an inhibitor of N-linked glycosylation and by the formation of *N*-glycosidic protein-carbohydrate linkages.[26] It specifically inhibits dolichol pyrophosphate-mediated glycosylation of asparaginyl residues of glycoproteins,[27] accumulates the unfolded proteins, and induces ER stress.[25,28] To determine the intracellular mechanisms that induce Aβ accumulation in RPE, we treated human retinal pigment epithelial cells, ARPE19 cells, with various ER-stress inducers, such as TM and TG, and investigated the responses of the Aβ accumulation-inducible event.

Materials and Methods

Cell Culture

ARPE19 cells were purchased from the American Type Culture Collection (ATCC, Manassas, VA) and were cultured in Dulbecco modified Eagle medium/F-12 human amniotic membrane nutrient mixture (DMEM/F-12; Sigma-Aldrich, St. Louis, MO) with 10% fetal bovine serum (FBS; Sigma-Aldrich) in a humidified incubator at 37°C in an atmosphere of 5% CO_2. The medium was changed every 3 days.

Preparation of Reagents

TG (Sigma-Aldrich) was dissolved in dimethyl sulfoxide (DMSO; Sigma-Aldrich) at a concentration of 0.5 mM to produce stock solutions. These solutions were diluted to 1:500 with medium to obtain 1 μM TG-containing culture medium. To evaluate the effect of DMSO, medium containing only DMSO (1:500 of total volume) was also prepared for each study. In comparison with TG, 1 μM TM (Sigma-Aldrich) and 0.1 μM staurosporine (STS; Sigma-Aldrich), the bacterial alkaloid that did not induce apoptosis through the ER,[29] were used for each study. Both TG and TM were reported to upregulate *VEGF* mRNA expression in ARPE19 cells.[30] The concentrations of TG and TM used to treat ARPE19 cells were the ones that induced *VEGF* mRNA expression maximally in all experiments in this study. The concentration of STS was selected based on a previous paper.[31] Every reagent was exposed to the ARPE19 cells for 24 hours.

RNA Isolation and cDNA Preparation

Total RNA from ARPE19 cells with exposure to each reagent was isolated (RNA Easy Kit; Qiagen, Tokyo Japan) and quantified by ultraviolet spectrometry at 260 nm. One microgram of RNA was transcribed to cDNA using reverse transcription reagents (Superscript III; Invitrogen, Carlsbad, CA).

Real-Time RT-PCR

Real-time RT-PCR was performed on a thermocycler (7900HT Sequence Detection Systems; Applied Biosystems, Foster, CA) with nuclear stain (SYBR Green; Applied Biosystems) reagents according to the manufacturer's instructions. Amplification of PCR products was measured by fluorescence associated with binding of double-stranded DNA to the SYBR green dye in the reaction mixture. Sequences of the primers used in this study are listed in Table 1. After an initial denaturation step of 50°C for 2 minutes and 95°C for 10 minutes, PCR involved 40 cycles at 95°C for 15 seconds and at 60°C for 1 minute. Quantification of each PCR product was expressed relative to GAPDH.

RT-PCR

For semiquantitative experiments, each PCR amplification was tested to reach half the saturation curve, and an aliquot of cDNA libraries was amplified by PCR with specific oligonucleotides for *APP* isoforms *APP770*, *APP751*, and *APP695* (605, 586, and 418 bp, respectively, of PCR product). APP primers were designed to flank the alternatively spliced exons (exons 7 and 8) to detect the expression of the three major APP isoforms found in the brain. Oligonucleotide sequences used were as follows: sense, 5′-aga gag aac cac cag cat tgc c-3′ (992–1013 bp); antisense, 5′-ggt cat tga gca tgg ctt cca c-3′ (1575–1596). These sequences were designed from the human APP cDNA sequences corresponding to GenBank accession number NM_000484. Amplification was performed in a thermocycler (PCR System 9700; Applied Biosystems). Conditions of amplification were 30 seconds at 95°C, 30 seconds at 57°C, and 1 minute at 72°C for 28 cycles to detect *APP770* and *APP751* or for 33 cycles to detect *APP695*. Finally, 5% polyacrylamide gels were stained by ethidium bromide and acquired with a CCD camera. mRNA levels were quantified using NIH image and normalized to the GAPDH levels.

Western Blot

Cells were homogenized in lysis buffer (10 mM Tris-HCl [pH 8.0], 1 mM EDTA, 150 mM NaCl, 0.5% NP-40) and were stored in sample buffer (50 mM TBS containing 2% sodium dodecyl sulfate [SDS], 6% β-mercaptoethanol, 10% glycerol) at −20°C until use. Quantification of the protein contents was made by the Bradford method.

Protein samples (15 μg) were separated on SDS-PAGE (12% acrylamide) and were transferred to polyvinylidene difluoride filters (Millipore, Bedford, MA). The filters were blocked in 0.1 M PBS containing 5% skim milk and 0.05% Tween 20 for 1 hour at room temperature and were incubated overnight at 4°C with a monoclonal mouse anti-

Table 1. Primer Sequences Used in This Study

Gene	Oligo Name	Sequence	Accession No.
APP	Forward	ctg gcc ctg gag aac tac atc a	NM_000484
	Reverse	gcg cgg aca tac ttc ttt agc a	
BACE	Forward	tca ccc aag gtc acc aaa caa c	NM_012104
	Reverse	tga agt cct cac cct ttc cca t	
caspase-4	Forward	ctg aag gac aaa ccc aag gtc a	U25804
	Reverse	cac ttc caa gga tgc tgg aga g	
ECE	Forward	aac tcc aac agc aac gtg atc c	NM_001397
	Reverse	cgg tca gca cct tct cgt ttt	
GAPDH	Forward	cac tga atc tcc cct cct cac a	NM_002046
	Reverse	tga tgg tac atg aca agg tgc g	
neprilysin	Forward	cat cgg cat ggt cat agg aca	NM_007287
	Reverse	tgt tga gtc cac cag tca acg a	
PEDF	Forward	gcc agg tcc aca aag gaa att	AF_400442
	Reverse	aac ttt gtt acc cac tgc ccc	
TACE	Forward	ttc act gga cac gtg gtt ggt	NM_002046
	Reverse	ggc ccc atc tgt gtt gat tct	
TNF-α	Forward	aac aac cct cag acg cca cat	NM_000594
	Reverse	cag tgc tca tgg tgt cct ttc c	
VEGF	Forward	aag aag cag ccc atg aca gct	NM_001025366
	Reverse	tag gtc ctt tta ggc tgc acc c	

caspase-4 (1:1000; MBL, Nagano Japan) and a polyclonal rabbit anti-VEGF (1:200; Santa Cruz Biotechnology, Santa Cruz, CA) primary antibody. After five washes in 0.1 M PBS containing 0.05% Tween 20, the filters were incubated for 1 hour at room temperature with a horseradish peroxidase (HRP)-conjugated anti-mouse IgG (1:1000; Cell Signaling, Beverly, MA) and an anti-rabbit IgG (1:1000; Cell Signaling) secondary antibody, washed, visualized in ECL solution (Amersham Biosciences, Arlington Heights, IL) for 10 minutes, and exposed onto film (X-Omat; Fuji, Kanagawa, Japan) for 7 to 10 minutes. Finally, the filters were incubated in a stripping buffer (2% SDS, 0.7% β-mercaptoethanol, 62.5 mM Tris-HCl, pH 6.8) for 30 minutes at 65°C and were reprobed with a monoclonal mouse anti-β-actin antibody (1:3000; Chemicon, Temecula, CA) as loading controls. Our Western blot bands showed the same band sizes as indicated in the antibody information sheets. Protein levels were quantified by densitometry and normalized to the β-actin levels.

Data and Statistical Analyses

Statistical analysis of mRNA and protein expression levels for each reagent treatment was performed using the Student's *t*-test in comparisons with DMSO treatment (control). Data were expressed as mean ± SE ($n = 3$).

Intracellular Ca^{2+} Measurement

The intracellular Ca^{2+} concentration in retinal pigment epithelial cells was monitored using the Ca^{2+} indicator dye (Fluo-4; Invitrogen). After 3 days in vitro, cells were incubated for 20 minutes with the cell-permeant acetomethyl ester form of 5 mM Ca^{2+} indicator dye (Fluo-4; Invitrogen) diluted in culture medium containing 0.01% pluonic acid F-127 at 37°C. The cells were subsequently washed three times with culture medium, and the dye was allowed to deesterify for an additional 30 minutes in the CO_2 incubator. Ca^{2+} imaging experiments were performed using a live cell imaging microscope system (BioStation IM; Nikon, Tokyo, Japan) with a 20× objective. Fluorescent images were acquired every 20 seconds. Fluo-4 fluorescence was produced by excitation from a 130-W mercury-vapor lamp and an appropriate filter set (B-2A [Nikon]; excitation, 450–490 nm; emission, 520–560 nm; dichroic, 510 nm). All drugs were applied by bath application after 5-minute control observation. Data analysis was performed as follows: off-line analysis of the images was performed using commercial software (Aquacosmos; Hamamatsu Photonics, Hamamatsu, Japan). Fluorescence signal was quantified by measuring the average pixel intensity within cell bodies. Changes in fluorescence intensity of each cell were normalized to its baseline fluorescence intensity.

Results

Induction of Aβ Production-Inducible APP Splice Variants mRNA Expression in ER-Stress–Treated ARPE19 Cells

In the amyloidogenic pathway, the cleavage of APP by the β-secretase and presenilin complex results in Aβ production. *APP* has several splice variants. Exons 7, 8, and 15 of the *APP* gene can be alternatively spliced to produce multiple isoforms. In the brain, the major isoform transcripts result from the splicing of exons 7 and 8, which gives rise to APP695, APP751, and APP770.[20] Both APP770 and APP751 contain a serine protease inhibitory domain encoded by exon 7 called the Kunitz protease inhibitory domain (KPI). KPI-APP has been shown to be more amyloidogenic than KPI-deficient APP.[32]

In the ARPE19 cells, the exposure of TG, which induces a depletion of intracellular Ca stores, slightly increased the expression of *KPI-APP*, such as *APP751* and *APP770* (Fig. 1A). TM, which inhibits N-linked glycosylation, induced an increase of *KPI-APP* expression in ARPE19 cells (Fig. 1A). STS, which is widely used as an inducer of non-ER stress-induced apoptosis, did not induce the expression of *KPI-APP* (Fig. 1A). Real-time RT-PCR showed no change in the total *APP* mRNA expression of any of the reagent treatments (Fig. 1B). These results indicate that ER stress induces mRNA expression of *APP* splice variants, which accelerate Aβ accumulation, in ARPE19 cells.

Decrease of Aβ Metabolism-Related Factors mRNA Expression in TG-Treated ARPE19 Cells

To find the relationship between ER stress-inducing factors and cellular mRNA expression of a series of Aβ metabolism-related factors (such as neprilysin, ECE, and BACE) in ARPE19 cells, we performed real-time RT-PCR.

TG-treated ARPE19 cells showed a remarkable decrease in mRNA expression of neprilysin, which highly degrades $A\beta^{35-34}$ (Fig. 2A). The mRNA expression of *ECE*, which degrades Aβ, and of *BACE*, which cleaves APP at the β site, was not quantitatively changed by TG (Figs. 2B, 2C). The expression of all investigated Aβ metabolism-related genes were not affected by TM or STS treatment (Fig. 2). Because there was a remarkable

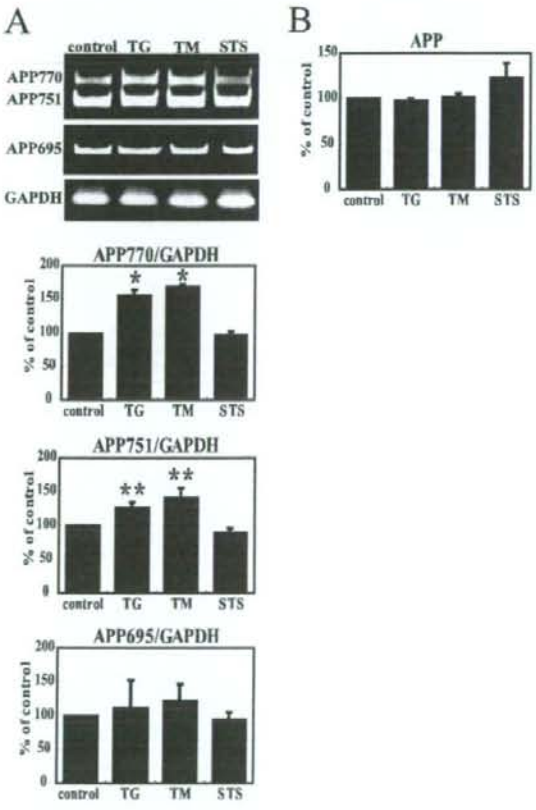

FIGURE 1. (A) Transcriptional expression of APP isoforms in cultured ARPE19 cells induced by TG, TM, and STS by RT-PCR analysis and densitometric analyses. Data are expressed as the mean ± SE ($n = 5$). The results show that TG and TM treatment induced a slight increase in *APP751* and *APP770* but not *APP695* compared with the control. $^{**}P < 0.05$ and $^{*}P < 0.01$ for comparison with the control, by Student's *t*-test. (B) Expression of *APP* mRNA induced by TG, TM, and STS using real-time RT-PCR analysis. Data are expressed as mean ± SE ($n = 5$). Expression of *APP* did not change in all ARPE19 cell samples compared with the control. $^{*}P < 0.01$ for comparison with the control, by Student's *t*-test.

decrease of neprilysin mRNA observed in only TG-treated cells, it is suggested that the degradation of Aβ is depressed by a decrease in the expression of neprilysin in ARPE19 cells.

Induction of Angiogenic Factors mRNA Expression in ER-Stress–Treated ARPE19 Cells

It has been reported that exposure to Aβ induced the mRNA expression of *VEGF* and a reduction of *PEDF* in ARPE19 cells.[12] We investigated the cellular mRNA expression change of *VEGF* and *PEDF* produced by TG and TM treatment in ARPE19 cells. In addition, real-time RT-PCR was performed for tumor necrosis factor alpha (*TNF-α*) and TNF-α converting enzyme (*TACE*). TNF-α, a macrophage/monocyte-derived polypeptide, stimulates VEGF production in human glioma cells and retinal pigment epithelial cells,[35,36] and TACE is involved the generation of soluble TNF-α from membrane-bound TNF-α and promotes angiogenesis.[37,38]

TG and TM exclusively upregulated *VEGF* mRNA expression, as reported previously,[30] as did STS (Fig. 3A). Real-time RT-PCR showed that TG and STS exclusively downregulated *PEDF* mRNA expression, and TM did not change (Fig. 3B). TG and TM also upregulated the mRNA expression of *TNF-α* and *TACE* (Figs. 3C, 3D). STS upregulated the mRNA expression of *TNF-α* but did not change that of *TACE* (Figs. 3C, 3D). To confirm the increase of VEGF expression at the protein level, we performed Western blot analysis for VEGF and showed that TG and TM also upregulated VEGF protein expression (Fig. 3E). These results suggest that the change in expression of these angiogenic factors might be the result of a general apoptotic event.

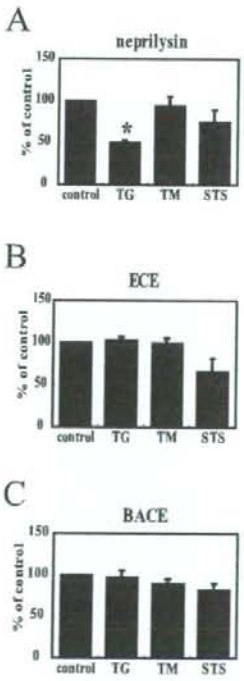

FIGURE 2. Expression of Aβ-metabolic process-related genes such as neprilysin (**A**), *ECE* (**B**), and *BACE* (**C**) mRNA induced by TG, TM, and STS using real-time RT-PCR analysis. Data are expressed as mean ± SE ($n = 3$). Expression of *ECE* (**B**) and *BACE* (**C**) did not change in all ARPE19 cells sample compared with the control. Expression of neprilysin (**A**) mRNA decreased in only TG-treated ARPE19 cells compared with the control. $^{*}P < 0.01$ for comparison with the control, by Student's *t*-test.

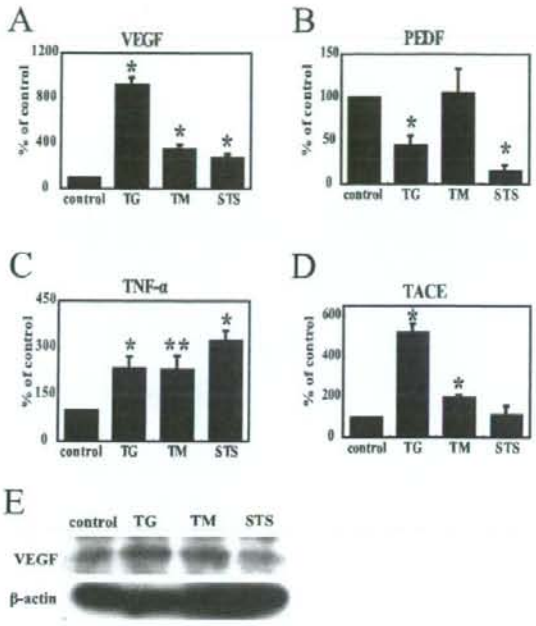

FIGURE 3. Expression of angiogenesis-related genes such as *VEGF* (**A**), *PEDF* (**B**), *TNF-α* (**C**), and *TACE* (**D**) induced by TG, TM, and STS using real-time RT-PCR analysis. Data are expressed as mean ± SE ($n = 3$). Graphs show the upregulation of *VEGF* (**A**), *TNF-α* (**C**), and mRNA in all ARPE19 cell samples compared with the control. Expression of *PEDF* (**B**) decreased in TG- and STS-induced ARPE19 cell mRNA compared with the control. Expression of *TACE* (**D**) increased in TG- and TM-induced ARPE19 cell mRNA compared with the control. $^{**}P < 0.05$ and $^{*}P < 0.01$ for comparison with the control, by Student's *t*-test (**E**) Expression of VEGF protein induced by TG, TM, and STS using Western blot. Results show the upregulation of VEGF as it was affected by TG and TM compared with the control. These data were confirmed by three independent Western blot analyses.

Induction of Caspase-4 Expression in TG-Treated ARPE19 Cells

Caspase-4 is primarily activated in ER stress-induced apoptosis.[39] Real-time RT-PCR and Western blot showed that the expression of caspase-4 mRNA and the active form of its protein were upregulated by TG treatment (Fig. 4). Although expression of the active form of caspase-4 protein was also upregulated by TM treatment, it was much lower than that of TG-treated ARPE19 cells (Fig. 4). STS-treated ARPE19 cells showed no change in expression of caspase-4 (Fig. 4).

Induction of Intracellular Ca Elevation in TG-Treated ARPE19 Cells

TG can inhibit the sarcoplasmic reticulum calcium-ATPase and can elevate intracellular Ca concentration.[23] We performed Ca imaging (Fluo-4 and Fura-2/AM; Invitrogen) to investigate whether the intracellular Ca concentration was actually increased in TG-treated ARPE19 cells. TG-treated ARPE19 cells showed a remarkable increase in intracellular Ca concentration (Fig. 5 and Supplementary Fig. S1, online at http://www.iovs.org/cgi/content/full/49/6/2376/DC1). TM- and STS-treated

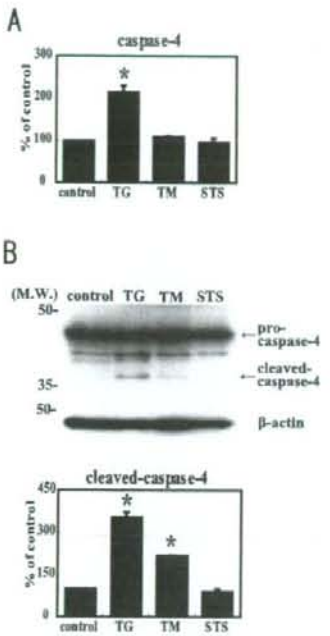

FIGURE 4. (A) Expression of caspase-4 induced by TG, TM, and STS using real-time RT-PCR analysis. The graph shows the upregulation of caspase-4 mRNA as it was affected by TG compared with the control. (B) Expression of the active-form of caspase-4 (cleaved-caspase-4) induced by TG, TM, and STS using Western blot and densitometric analyses. Results show the activation of caspase-4 as it was affected by TG and TM compared with the control. Data are expressed as mean ± SE ($n = 3$). $^*P < 0.01$ for comparison with the control, by Student's *t*-test.

ARPE19 cells showed no change in intracellular Ca concentration (Fig. 5 and Supplementary Fig. S1).

DISCUSSION

Recently, it has been reported that Aβ accumulates in the RPE of patients with AMD,[4–5] which is the most common cause of vision loss in the development of CNV. Aβ, known as the hallmark of AD, is routinely produced in the normal brain and is readily degraded by catabolic enzymes. However, facilitation of Aβ production is caused by mutation of the gene responsible for AD. Aβ then accumulates as the insoluble senile plaques in the brain. ER stress is considered one of the causative factors for the accumulation of Aβ in AD.[40] To examine the intracellular machinery for Aβ accumulation in the RPE of patients with AMD, we treated human retinal pigment epithelial cells, ARPE19 cells, with the ER-stress inducer and investigated whether Aβ accumulation was inducible. Our results suggested that Aβ accumulation-inducible factors were induced by ER stress in retinal pigment epithelial cells as well as in neural cells, and angiogenic factors were additively increased in retinal pigment epithelial cells by ER stress under the same conditions.

We showed that ER stress treatment induced an increase in mRNA expression of Aβ production-inducible *APP* splice variants; only TG treatment further induced a decrease in the mRNA expression of neprilysin in ARPE19 cells (Figs. 1, 2). It has been reported that KPI-APP, which increases at the mRNA level in the brains of persons with AD,[41] is more amyloidogenic than KPI-deficient APP.[42] Therefore, it is thought that the increase in mRNA expression of KPI-APP induced the production of Aβ. On the other hand, neprilysin knockout mice have been reported to display an approximately 50% increase in the levels of Aβ40 and Aβ42.[14] Based on these facts, we surmised that the increased Aβ production and the decreased Aβ degradation induced specifically by TG treatment in ARPE19 cells might be attributed to the Aβ accumulation in ARPE19 cells.

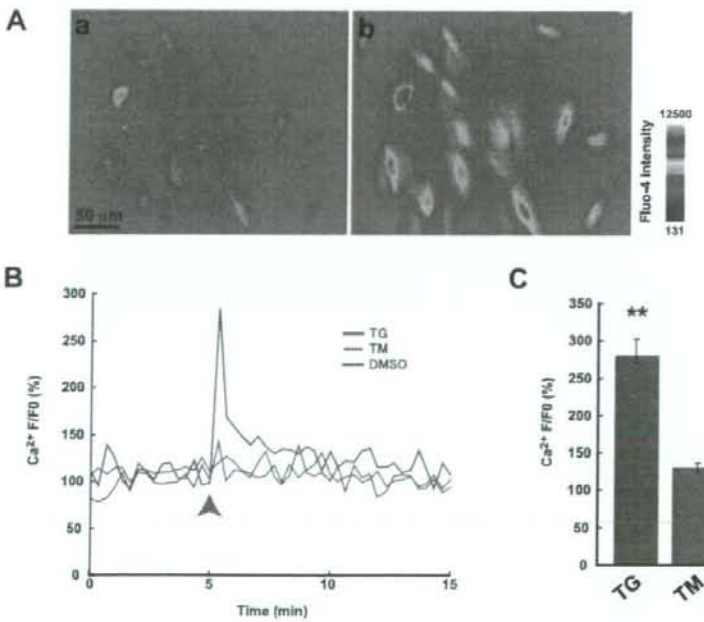

FIGURE 5. Effects of TG and TM on Ca^{2+} elevation in retinal pigment epithelial cell soma. (A) A representative experiment showing that TG (1 μM) evoked increases in cytosolic Ca^{2+}. These images are pseudocolor images of Ca^{2+} indicator dye fluorescence (**a**, 0 min; **b**, 20 seconds after TG application). Scale bar, 50 mm. (B) Representative traces showing the average changes in Ca^{2+} indicator dye fluorescence of the retinal pigment epithelial cells. Spontaneous Ca^{2+} elevations were also observed in retinal pigment epithelial cells before the application of drugs. Note that the application of TG rapidly and markedly increased Ca^{2+} indicator dye fluorescence. (C) Average amplitudes of first peaks after drug application. Note that TG significantly increased the peak amplitude of Ca^{2+} elevation but that TM did not. Statistical differences were established using the Mann-Whitney *U* test at $^{**}P < 0.01$ ($n = 34–58$). Error bars indicate SEMs.

We also confirmed that the upregulation of *TNF-α*, *TACE*, and *VEGF* and the downregulation of *PEDF* were induced by TG treatment in ARPE19 cells at the mRNA level (Figs. 3A–D). Moreover, VEGF protein expression was upregulated by TG treatment (Fig. 3E), suggesting that TG treatment induced the expression not only of Aβ accumulation-promoting factor expression but also of angiogenic factors in ARPE19 cells.

Because transcription factor 4, activated by ER stress, induced VEGF,[42] ER stress has been considered to induce not only Aβ accumulation but also angiogenesis. However, our results showed a pronounced difference in the responses of Aβ accumulation-promoting factors and angiogenic factors between TG and TM, likely because of two reasons. First, there was a difference in the extent of ER stress-induced apoptosis. Caspase-4, which is primarily activated in ER stress-induced apoptosis,[39] was shown to be activated in TG-treated ARPE19 cells more than in TM-treated ARPE19 cells (Fig. 4). Second, we conjectured that the difference in results was attributed to the mechanism of action of each ER stress inducer. TG-induced ER stress was caused by the depletion of intracellular Ca stores,[24] whereas TM-induced ER stress was caused by an inhibition of N-linked glycosylation.[28] Differing from both TM- and STS-treated ARPE19 cells, we showed TG-treated ARPE19 cell exhibited striking increases in intracellular Ca concentration. It has been reported that insulin-like growth factor-1 stimulates increased VEGF secretion through the induction of the second messenger Ca in ARPE19 cells.[43] The elevation of intracellular Ca levels was also reported to increase Aβ peptide production through the activation of a protease, which requires Ca, in the cultured cells.[44] Based on these facts, intracellular increases of Ca by TG treatment may induce Aβ accumulation and angiogenic factors in ARPE19 cells more effectively than ER stress induced by TM.

It has long been known that the elevation of intracellular free calcium by TG has cytotoxic consequence in many cells (adipocytes,[45] T lymphocytes,[46] parotid acinar cells,[47] and peritoneal macrophages[48]) and cell lines (hepatocytes,[49] HeLa cells,[50] and NG115-401L cells[24]), including ARPE19 cells.[51] TM was used mainly for analysis in N-glycosylation (except that TM was used as an ER-stress inducer), whereas TG is involved in various cellular functions, including platelet activation,[52] inflammation,[53] skin irritation,[54] protein synthesis inhibition in human hepatoma cells,[55] vascular contractility,[56] and tumor promotion.[55] Moreover, it has been reported that TG induced Bax activation and was involved in mitochondrial caspase-dependent death.[57] It was often said that the low concentrations (0.5–2 μM) of TG increased the intracellular Ca and high concentration (1–10 μM) of TG-induced apoptosis (refer to Sigma data sheet). In addition, it has been reported that long-term (48-hour) exposure of TG led to recovery from upregulation of the intracellular Ca concentration[58] and the induction of cell death.[49] In our study, TG was exposed at 1 μM for 24 hours because we wanted to determine the change of various factors in the viable retinal pigment epithelial cells at early stages of Aβ accumulation. Our results were consistent with those of a previous report[51] in the elevation of the intracellular Ca concentration (Fig. 5). However, the change of BAX expression was not induced, probably because of the lower concentration and shorter incubation time of TG (data not shown). Therefore, TG would induce Aβ accumulation and angiogenic responses in retinal pigment epithelial cells mainly through induction of the intracellular Ca concentration in this study. Further studies would be needed to determine the responses under various conditions of TG incubation.

It has been reported that neprilysin inhibits angiogenesis through the proteolysis of fibroblast growth factor-2 (FGF-2),[59] and neprilysin knockout mice display an upregulation of VEGF and a downregulation of PEDF in their RPE.[12] Therefore, it is possible that the reduction of neprilysin mRNA expression induces angiogenesis. VEGF, which increases in AD patients, binds to Aβ with high affinity,[60] and Aβ stimulates the angiogenic response through FGF-2.[61] In addition, Aβ-treated ARPE19 cells display an upregulation of VEGF and a downregulation of PEDF.[12] Taken together, these reports suggest the possibility that Aβ induces angiogenesis. However, in our study, it was unclear whether Aβ or neprilysin directly affected angiogenesis because the stress-inducer treatment time was short.

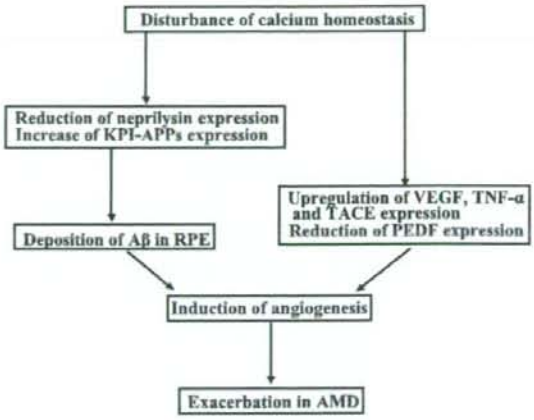

FIGURE 6. Display of the hypothesis that the disturbances in Ca homeostasis involve the pathogenic mechanism of AMD.

In the present study, we demonstrated that ER stress could cause the promotion of Aβ accumulation-inducible and angiogenic factors at the mRNA level in ARPE19 cells. Moreover, we showed that TG induced those factors more effectively than TM. Therefore, we propose that TG treatment produced an elevation of the intracellular Ca concentration, which was one of the responsible factors for the onset or acceleration of Aβ accumulation and angiogenesis in the retinal pigment epithelial cultured cells. Because Aβ exists in the RPE of patients with AMD and caused a disruption of cellular Ca homeostasis,[62,63] we speculate that intracellular Ca homeostasis disturbance in RPE may be involved in one of the pathogenic mechanism of AMD (Fig. 6). Detailed analysis of the intracellular responses of ARPE19 cells to TG might be useful for the mechanism of AMD.

References

1. Ambati J, Ambati BK, Yoo SH, Ianchulev S, Adamis AP. Age-related macular degeneration: etiology, pathogenesis, and therapeutic strategies. *Surv Ophthalmol*. 2003;48:257–293.
2. Gass JD. Drusen and disciform macular detachment and degeneration. *Trans Am Ophthalmol Soc*. 1972;70:409–436.
3. Johnson LV, Leitner WP, Rivest AJ, et al. The Alzheimer's A beta-peptide is deposited at sites of complement activation in pathologic deposits associated with aging and age-related macular degeneration. *Proc Natl Acad Sci U S A*. 2002;99:11830–11835.
4. Dentchev T, Milam AH, Lee VM, Trojanowski JQ, Dunaief JL. Amyloid-beta is found in drusen from some age-related macular degeneration retinas, but not in drusen from normal retinas. *Mol Vis*. 2003;9:184–190.
5. Anderson DH, Talaga KC, Rivest AJ, et al. Characterization of beta amyloid assemblies in drusen: the deposits associated with aging and age-related macular degeneration. *Exp Eye Res*. 2004;78:243–256.
6. Ohno-Matsui K, Morita I, Tombran-Tink J, et al. Novel mechanism for age-related macular degeneration: an equilibrium shift between

the angiogenesis factors VEGF and PEDF. *J Cell Physiol.* 2001;189:323–333.
7. Duh EJ, Yang HS, Haller JA, et al. Vitreous levels of pigment epithelium-derived factor and vascular endothelial growth factor: implications for ocular angiogenesis. *Am J Ophthalmol.* 2004;137:668–674.
8. Campochiaro PA, Hackett SF. Ocular neovascularization: a valuable model system. *Oncogene.* 2003;22:6537–6548.
9. Witmer AN, Vrensen GF, Van Noorden CJ, Schlingemann RO. Vascular endothelial growth factors and angiogenesis in eye disease. *Prog Retin Eye Res.* 2003;22:1–29.
10. Dawson DW, Volpert OV, Gillis P, et al. Pigment epithelium-derived factor: a potent inhibitor of angiogenesis. *Science.* 1999;285:245–248.
11. Tombran-Tink J, Shivaram SM, Chader GJ, Johnson LV, Bok D. Expression, secretion, and age-related downregulation of pigment epithelium-derived factor, a serpin with neurotrophic activity. *J Neurosci.* 1995;15:4992–5003.
12. Yoshida T, Ohno-Matsui K, Ichinose S, et al. The potential role of amyloid beta in the pathogenesis of age-related macular degeneration. *J Clin Invest.* 2005;115:2793–2800.
13. Saido TC. Alzheimer's disease as proteolytic disorders: anabolism and catabolism of beta-amyloid. *Neurobiol Aging.* 1998;19:S69–S75.
14. Iwata N, Tsubuki S, Takaki Y, et al. Metabolic regulation of brain Aβ by neprilysin. *Science.* 2001;292:1550–1552.
15. Selkoe DJ. Alzheimer's disease: genes, proteins, and therapy. *Physiol Rev.* 2001;81:741–766.
16. Vassar R, Bennett BD, Babu-Khan S, et al. Beta-secretase cleavage of Alzheimer's amyloid precursor protein by the transmembrane aspartic protease BACE. *Science.* 1999;286:735–741.
17. Takasugi N, Tomita T, Hayashi I, et al. The role of presenilin cofactors in the gamma-secretase complex. *Nature.* 2003;422:438–441.
18. Iwata N, Takaki Y, Fukami S, Tsubuki S, Saido TC. Region-specific reduction of A beta-degrading endopeptidase, neprilysin, in mouse hippocampus upon aging. *J Neurosci Res.* 2002;70:493–500.
19. Eckman EA, Reed DK, Eckman CB. Degradation of the Alzheimer's amyloid beta peptide by endothelin-converting enzyme. *J Biol Chem.* 2001;276:24540–24548.
20. Selkoe DJ. Amyloid beta-protein and the genetics of Alzheimer's disease. *J Biol Chem.* 1996;271:18295–18298.
21. Wong WL, Brostrom MA, Kuznetsov G, Gmitter-Yellen D, Brostrom CO. Inhibition of protein synthesis and early protein processing by thapsigargin in cultured cells. *Biochem J.* 1993;289(pt 1):71–79.
22. Sato N, Imaizumi K, Tohyama M, et al. Increased production of β-amyloid and vulnerability to endoplasmic reticulum stress by an aberrant spliced form of presenilin 2. *J Biol Chem.* 2001;276:2108–2114.
23. Treiman M, Caspersen C, Christensen SB. A tool coming of age: thapsigargin as an inhibitor of sarco-endoplasmic reticulum Ca^{2+}-ATPases. *Trends Pharmacol Sci.* 1998;19:131–135.
24. Jackson TR, Patterson SI, Thastrup O, Hanley MR. A novel tumour promoter, thapsigargin, transiently increases cytoplasmic free Ca^{2+} without generation of inositol phosphates in NG115-401L neuronal cells. *Biochem J.* 1988;253:81–86.
25. Lee AS. The glucose-regulated proteins: stress induction and clinical applications. *Trends Biochem Sci.* 2001;26:504–510.
26. Mahoney WC, Duksin D. Biological activities of the two major components of tunicamycin. *J Biol Chem.* 1979;254:6572–6576.
27. Olden K, Pratt RM, Jaworski C, Yamada KM. Evidence for role of glycoprotein carbohydrates in membrane transport: specific inhibition by tunicamycin. *Proc Natl Acad Sci U S A.* 1979;76:791–795.
28. Patil C, Walter P. Intracellular signaling from the endoplasmic reticulum to the nucleus: the unfolded protein response in yeast and mammals. *Curr Opin Cell Biol.* 2001;13:349–355.
29. Mao YW, Liu JP, Xiang H, Li DW. Human αA- and αB-crystallins bind to Bax and Bcl-X(S) to sequester their translocation during staurosporine-induced apoptosis. *Cell Death Differ.* 2004;11:512–526.
30. Abcouwer SF, Marjon PL, Loper RK, Vander, Jagt DL. Response of VEGF expression to amino acid deprivation and inducers of endoplasmic reticulum stress. *Invest Ophthalmol Vis Sci.* 2002;43:2791–2798.
31. John PM, Neville NO. Induction of apoptosis in cultured human retinal pigmented epithelial cells the effect of protein kinase c activation and inhibition. *Neurochem Int.* 1997;31:261–275.
32. Ho L, Fukuchi K, Younkin SG. The alternatively spliced Kunitz protease inhibitor domain alters amyloid beta protein precursor processing and amyloid beta protein production in cultured cells. *J Biol Chem.* 1996;271:30929–30934.
33. Shirotani K, Tsubuki S, Iwata N, et al. Neprilysin degrades both amyloid beta peptides 1–40 and 1–42 most rapidly and efficiently among thiorphan- and phosphoramidon-sensitive endopeptidases. *J Biol Chem.* 2001;276:21895–21901.
34. Takaki Y, Iwata N, Tsubuki S, et al. Biochemical identification of the neutral endopeptidase family member responsible for the catabolism of amyloid beta peptide in the brain. *J Biochem (Tokyo).* 2000;128:897–902.
35. Ryuto M, Ono M, Izumi H, et al. Induction of vascular endothelial growth factor by tumor necrosis factor alpha in human glioma cells: possible roles of SP-1. *J Biol Chem.* 1996;271:28220–28228.
36. Oh H, Takagi H, Takagi C, et al. The potential angiogenic role of macrophages in the formation of choroidal neovascular membranes. *Invest Ophthalmol Vis Sci.* 1999;40:1891–1898.
37. Black RA, Rauch CT, Kozlosky CJ, et al. A metalloproteinase disintegrin that releases tumour-necrosis factor-alpha from cells. *Nature.* 1997;385:729–733.
38. Moss ML, Jin SL, Milla ME, et al. Cloning of a disintegrin metalloproteinase that processes precursor tumour-necrosis factor-alpha. *Nature.* 1997;385:733–736.
39. Hitomi J, Katayama T, Eguchi Y, et al. Involvement of caspase-4 in endoplasmic reticulum stress-induced apoptosis and Aβ-induced cell death. *J Cell Biol.* 2004;165:347–356.
40. Katayama T, Imaizumi K, Manabe T, et al. Induction of neuronal death by ER stress in Alzheimer's disease. *J Chem Neuroanat.* 2004;28:67–78.
41. Preece P, Virley DJ, Constandi M, et al. Amyloid precursor protein mRNA levels in Alzheimer's disease brain. *Brain Res Mol Brain Res.* 2004;122:1–9.
42. Ameri K, Harris AL. Activating transcription factor 4. *Int J Biochem Cell Biol.* 2008;40:14–21.
43. Rosenthal R, Wohlleben H, Malek G, et al. Insulin-like growth factor-1 contributes to neovascularization in age-related macular degeneration. *Biochem Biophys Res Commun.* 2004;323:1203–1208.
44. Querfurth HW, Selkoe DJ. Calcium ionophore increases amyloid beta peptide production by cultured cells. *Biochemistry.* 1994;33:4550–4561.
45. Begum N, Leitner W, Reusch JE, Sussman KE, Draznin B. GLUT-4 phosphorylation and its intrinsic activity: mechanism of Ca(2+)-induced inhibition of insulin-stimulated glucose transport. *J Biol Chem.* 1993;268:5552–5556.
46. Gouy H, Cefai D, Christensen SB, Debre P, Bismuth G. Ca^{2+} influx in human T lymphocytes is induced independently of inositol phosphate production by mobilization of intracellular Ca^{2+} stores: a study with the Ca^{2+} endoplasmic reticulum-ATPase inhibitor thapsigargin. *Eur J Immunol.* 1990;20:2269–2275.
47. Takemura H, Hughes AR, Thastrup O, Putney JW Jr. Activation of calcium entry by the tumor promoter thapsigargin in parotid acinar cells. *J Biol Chem.* 1989;264:12266–12271.
48. Ohuchi K, Sugawara T, Watanabe M, et al. Analysis of the stimulative effect of thapsigargin, a non-TPA-type tumour promoter, on arachidonic acid metabolism in rat peritoneal macrophages. *Br J Pharmacol.* 1988;94:917–923.
49. Canova NK, Kmonickova E, Martinek J, Zidek Z, Farghali H. Thapsigargin, a selective inhibitor of sarco-endoplasmic reticulum Ca 2-ATPases, modulates nitric oxide production and cell death of primary rat hepatocytes in culture. *Cell Biol Toxicol.* 2007;23:337–354.
50. Middleton JP, Albers FJ, Dennis VW, Raymond JR. Thapsigargin demonstrates calcium-dependent regulation of phosphate uptake in HeLa cells *Am J Physiol.* 1990;259:F727–F731.

51. Reigada D, Lu W, Zhang X, et al. Degradation of extracellular ATP by the retinal pigment epithelium. *Am J Physiol Cell Physiol*. 2005;289:617–624.
52. Thastrup O, Linnebjerg H, Bjerrum PJ, Knudsen JB, Christensen SB. The inflammatory and tumor-promoting sesquiterpene lactone, thapsigargin, activates platelets by selective mobilization of calcium as shown by protein phosphorylations. *Biochim Biophys Acta*. 1987;927:65–73.
53. Ali H, Christensen SB, Foreman JC, et al. The ability of thapsigargin and thapsigargicin to activate cells involved in the inflammatory response. *Br J Pharmacol*. 1985;85:705–712.
54. Hakii H, Fujiki H, Suganuma M, et al. Thapsigargin, a histamine secretagogue, is a non-12-O-tetradecanoylphorbol-13-acetate (TPA) type tumor promoter in two-stage mouse skin carcinogenesis. *J Cancer Res Clin Oncol*. 1986;111:177–181.
55. Wong WL, Brostrom MA, Kuznetsov G, Gmitter-Yellen D, Brostrom CO. Inhibition of protein synthesis and early protein processing by thapsigargin in cultured cells. *Biochem J*. 1993;289:71–79.
56. Low AM, Darby PJ, Kwan CY, Daniel EE. Effects of thapsigargin and ryanodine on vascular contractility: cross-talk between sarcoplasmic reticulum and plasmalemma. *Eur J Pharmacol*. 1993;230:53–62.
57. Chin TY, Lin HC, Kuo JP, Chueh SH. Dual effect of thapsigargin on cell death in porcine aortic smooth muscle cells. *Am J Physiol Cell Physiol*. 2007;292:383–395.
58. Humez S, Legrand G, Vanden-Abeele F, et al. Role of endoplasmic reticulum calcium content in prostate cancer cell growth regulation by IGF and TNFα. *J Cell Physiol*. 2004;201:201–213.
59. Goodman OB, Febbraio M, Simantov R, et al. Neprilysin inhibits angiogenesis via proteolysis of fibroblast growth factor-2. *J Biol Chem*. 2006;281:33597–33605.
60. Yang SP, Bae DG, Kang HJ, et al. Co-accumulation of vascular endothelial growth factor with β-amyloid in the brain of patients with Alzheimer's disease. *Neurobiol Aging*. 2004;25:283–290.
61. Cantara S, Donnini S, Morbidelli L, et al. Physiological levels of amyloid peptides stimulate the angiogenic response through FGF-2. *FASEB J*. 2004;15:1943–1945.
62. Mark RJ, Hensley K, Butterfield DA, Mattson MP. Amyloid beta-peptide impairs ion-motive ATPase activities: evidence for a role in loss of neuronal Ca^{2+} homeostasis and cell death. *J Neurosci*. 1995;15:6239–6249.
63. Mark RJ, Lovell MA, Markesbery WR, Uchida K, Mattson MP. A role for 4-hydroxynonenal, an aldehydic product of lipid peroxidation, in disruption of ion homeostasis and neuronal death induced by amyloid beta-peptide. *J Neurochem*. 1997;68:255–264.

Available online at www.sciencedirect.com
ScienceDirect
Neurochemistry International 52 (2008) 683–687
NEUROCHEMISTRY International
www.elsevier.com/locate/neuint

Presenilin-1 mutation activates the signaling pathway of caspase-4 in endoplasmic reticulum stress-induced apoptosis

Futoshi Yukioka [a,b,1], Shinsuke Matsuzaki [a,b,c,1,*], Keisuke Kawamoto [a,b], Yoshihisa Koyama [a,b], Junichi Hitomi [d], Taiichi Katayama [e], Masaya Tohyama [a,b,c]

[a] Department of Anatomy and Neuroscience, Graduate School of Medicine, Osaka University, 2-2 Yamadaoka, Suita, Osaka 565-0871, Japan
[b] The 21st Century COE program, Japan
[c] The Osaka-Hamamatsu Joint Research Center For Child Mental Development, Japan
[d] Department of Cell Biology, Harvard Medical School, 240 Longwood Avenue, Boston, MA 02115, USA
[e] Department of Anatomy and Neuroscience, Hamamatsu University School of Medicine, 1-20-1 Handayama, Hamamatsu, Shizuoka 431-3192, Japan

Received 3 July 2007; received in revised form 24 August 2007; accepted 30 August 2007
Available online 4 September 2007

Abstract

In the previous reports, we showed that the familial Alzheimer's disease (AD)-linked presenilin-1 (PS1) mutation induced the fragility to the endoplasmic reticulum (ER) stress and that caspase-4 mediates ER stress-induced- and β-amyloid induced-apoptotic signaling in human cells. These results suggest the involvement of ER stress and caspase-4 in the cell death observed in AD. In this report, we studied the activation of caspase-4 in the familial AD-linked PS1 mutation (ΔE9). Cleavage of caspase-4 under ER stress was enhanced by the overexpression of the familial AD-linked mutation (ΔE9), showing that caspase-4 is a key caspase involved in the apoptotic signaling of AD. We also showed that the overexpression of caspase-4 induced cleavage of caspase-9 and caspase-3 without releasing cytochrome-*c* from the mitochondria. Thus, caspase-4 activates downstream caspases independently of mitochondrial apoptotic signaling and this might contribute to the pathogenesis of AD.

To sum up our data, the familial AD-linked PS1 mutation accelerates the cleavage of caspase-4 under the ER stress and results in the activation of caspase-9 and caspase-3, apoptosis signal, without releasing cytochrome-*c*.

Keywords: Caspase-4; Caspase-3; Caspase-9; Familial AD-linked presenilin-1 mutation; ER stress; Mitochondria; Alzheimer's disease

1. Introduction

Missense mutations in the human presenilin-1 (PS1) gene, which are found on chromosome 14, cause early-onset familial Alzheimer's disease (AD) (Sherrington et al., 1995). We have shown that familial AD-linked PS1 mutations increase vulnerability to endoplasmic reticulum (ER) stress by altering the unfolded-protein response (UPR) (Katayama et al., 1999). Caspase-12 has been shown to be involved in signaling pathways specific to ER stress-induced apoptosis (Nakagawa et al., 2000; Yoneda et al., 2001). Pro-caspase-12, which is predominantly localized in the ER, is specifically cleaved by ER stress, and caspase-12-deficient mice show a reduced sensitivity to amyloid-β (Aβ) (Nakagawa et al., 2000), which induces neuronal cytotoxicity (Yankner et al., 1989). Thus, caspase-12 has been suggested to play a key role in the pathogenesis of AD. However, it has been controversial whether similar mechanisms are working in the human (Katayama et al., 1999; Rao et al., 2001; Fischer et al., 2002). In humans, although the caspase-12 gene is transcribed into mRNA, mature caspase-12 protein would not be produced because the gene is interrupted by a frame shift and a premature stop codon (Fischer et al., 2002). Thus, human caspase-12 does not function in ER stress-induced apoptosis such as in AD, although some other caspases with similar structures might substitute functionally for caspase-12 in the human. Recently,

* Corresponding author at: Department of Anatomy and Neuroscience, Graduate School of Medicine, Osaka University, 2-2 Yamadaoka, Suita, Osaka 565-0871, Japan. Tel.: +81 6 6879 3221; fax: +81 6 6879 3229.
E-mail address: s-matsuzaki@anat2.med.osaka-u.ac.jp (S. Matsuzaki).
[1] Contributed equally to this work.

0197-0186/$ – see front matter © 2007 Elsevier Ltd. All rights reserved.
doi:10.1016/j.neuint.2007.08.017

we have revealed that caspase-4 can function as an ER stress-induced caspase in humans and may be involved in pathogenesis of AD (Hitomi et al., 2004). However, little is known about the downstream actions of caspase-4, though caspase-3 and caspase-9 are suggested to exist downstream from caspase-12 (Morishima et al., 2002). In the present study, we found that the familial AD-linked PS1 mutation accelerates the cleavages of caspase-4 to induce neuronal death, showing that caspase-4 is involved in the pathogenesis of familial AD. We also showed that the activation of caspase-4 activates caspase-3 and caspase-9 without involving the cytochrome-*c* pathway.

2. Materials and methods

2.1. Chemicals and antibodies

We used the following antibodies: anti-caspase-4 mAb (4B9; MBL International Corporation, Nagoya, Japan), anti-caspase-3 mAb (Cell Signaling Technology, Beverly, MA), anti-cytochrome-*c* pAb (MBL International Corporation), anti-β-actin mAb (C4; CHEMICON International Inc., Temecula, CA), anti-caspase-9 mAb (5B4; MBL International Corporation), anti-PUMA pAb (Sigma–Aldrich, St. Louis, MO), HRP-conjugated anti-mouse IgG antibody (Cell Signaling Technology) and HRP-conjugated anti-rabbit IgG antibody (Cell Signaling Technology). All antibodies were diluted to PBS containing 0.05% Tween-20. The chemical reagents used in this experiment were tunicamycin, thapsigargin and staurosporine (Sigma–Aldrich).

2.2. Cell culture

SK-N-SH cells and COS-7 cells were cultured in α-MEM (Invitrogen, Carlsbad, CA) and DMEM (Invitrogen), respectively, both containing 10% FBS, at 37 °C under 5% CO_2. SK-N-SH neuroblastoma cell lines stably expressing wild-type PS1 or PS1ΔE9 have been described previously (Katayama et al., 1999).

2.3. cDNA cloning

The expression plasmids for caspase-4 tagged the FLAG sequence at the 3′ end (the resultant constructs were termed caspase-4-FLAG) and FLAG have been described previously (Hitomi et al., 2004). We constructed the pcDNA3.1 (+) expression vector (Invitrogen) carrying the full-length human *caspase-4* cDNA encoding 854 (NM_001225) amino acids fused in-frame with the GFP sequence at the 3′ end and GFP (the resultant constructs were termed caspase-4-GFP and GFP, respectively).

2.4. Subcellular fractionation

COS-7 cells cultured on a 10-cm dish were washed twice with PBS, harvested and suspended in buffer A (50 mM Tris–HCl, pH 8.0, 1 mM EDTA, 0.32 M sucrose, 0.1 mM PMSF) for 5 min on ice. Then the cells were passed through a 25-gauge needle 13 times and centrifuged at 500 × *g* for 10 min to collect a crude nuclear pellet. The supernatant was centrifuged at 1200 × *g* for 10 min to yield a mitochondria-enriched pellet and this supernatant was collected as a cytosolic fraction. The mitochondria-enriched pellets were dissolved in buffer A containing 0.3% triton. An equal volume of each fraction was subjected to Western blotting as described below, using the indicated antibodies.

2.5. Western blot analysis

Cells treated with the indicated reagents were washed twice with PBS, harvested, and lysed in TNE buffer (10 mM Tris–HCl, pH 7.8, 1 mM EDTA, 150 mM NaCl, 1 mM PMSF) containing 0.5% NP-40 and protease inhibitor cocktail (Roche, Sydney, Australia). Equal amounts of protein were subjected to 12% SDS-PAGE for caspase-4, caspase-9 and caspase-3 or 15% SDS-PAGE for cytochrome-*c* and transferred to a PVDF membrane (Millipore, Bedford, MA). The membrane was blocked with 5% skim milk and incubated with each primary antibody (anti-caspase-4 mAb, 1:1000; anti-caspase-9 mAb, 1:1000; anti-caspase-3 mAb, 1:1000; anti-cytochrome-*c* pAb, 1:200; anti-β-actin mAb, 1:2000; anti-PUMA pAb 1:1000) followed by incubation with an HRP-conjugated secondary antibody (anti-mouse IgG antibody, 1:1000; anti-rabbit IgG antibody, 1:1000). Proteins were visualized with an ECL detection system (Amersham Biosciences, Piscataway, NJ).

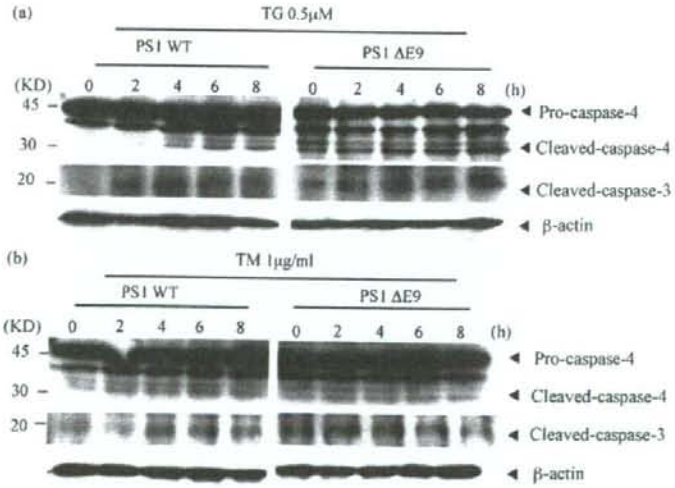

Fig. 1. FAD-linked mutation accelerates the cleavage of caspase-4 and caspase-3 under ER stress. SK-N-SH cells stably expressing PS1 (PS1WT) (a and b left panels) and mutant PS1 lacking exon 9 (PS1ΔE9) (a and b right panels) were treated with 0.5 μM thapsigargin (TG) (a) or 1 μg/ml tunicamycin (TM) (b) followed by incubation for indicated periods. Equal amounts of cell lysates were analyzed by Western blotting using anti-caspase-4 (upper panels of a and b), anti-caspase-3 (middle panels of a and b) or anti-β-actin (lower panels of a and b) antibody.

3. Results

3.1. PS1 mutation accelerated the cleavage of caspase-4 under ER stress

Familial AD-linked PS1 mutations, such as a deletion of exon 9 (PS1ΔE9), increase the vulnerability to ER stress by altering the UPR. ER stresses induce increased cell death in cells expressing mutant PS1 as compared with cells expressing the wild-type PS1. Caspase-4 and caspase-12 localized to the ER membrane are involved in the pathogenesis of neuronal death caused by ER stress in humans and rodents, respectively (Hitomi et al., 2004; Nakagawa et al., 2000). To determine the effect of PS1 mutation on the cleavage of caspases under ER stress, we studied the level of the cleavage of caspase-4 and caspase-3 after treatment with thapsigargin, an ER Ca-ATPase inhibitor, using wild-type PS1 or PS1ΔE9 expressing cells. Before thapsigargin treatment, we pretreated the cells with fresh medium for more than 1 h to obtain baseline data. After pre-incubation, the cells were exposed to 0.5 μM thapsigargin or 1 μg/ml tunicamycin. In wild-type PS1 cells, the cleaved form of caspase-4 and caspase-3 could not be identified under the basal condition and increased gradually after the addition of thapsigargin (Fig. 1a). In PS1ΔE9 cells, the cleaved forms of caspase-4 and caspase-3 were detected in the basal condition (Fig. 1a). The activation pattern of caspase-4 and caspase-3 under ER stress was correlated with each other, suggesting a close functional association between caspase-4 and caspase-3. The acceleration of the cleavage of caspase-4 and caspase-3 in PS1ΔE9 expressing cells were also induced by tunicamycin (Fig. 1b).

3.2. Caspase-4 induced the cleavage of caspase-9 and caspase-3

Next, we examined whether activation of caspase-4 induces the cleavage of caspase-3 or caspase-9. Caspase-4-FLAG or FLAG was overexpressed in COS-7 cells and there were effects of caspase-4 on the cleavage of caspase-3 and caspase-9. As a positive control of cleaved caspase-9 or caspase-3, the lysates of 0.1 μM staurosporin-treated COS-7 cells were used (Fig. 2b and c). Overexpression of caspase-4-FLAG, which caused the cleavage of caspase-4 in a self-(auto-)cleavage manner 24 h after overexpression of caspase-4-FLAG (Fig. 2a), induced remarkable cleavage of endogenous caspase-9 (Fig. 2b) and endogenous caspase-3 (Fig. 2c) in a concentration-dependent manner and such effects could not be detected in the control vector expressing cells (Fig. 2b and c). These results suggest that caspase-3 and capase-9 exist downstream from caspase-4.

3.3. Overexpression of caspase-4 did not affect on the efflux of cytochrome-c

Long exposure to ER stress influences mitochondrial function *via* PUMA (the Bcl-2 homology domain 3-only family member) (Reimertz et al., 2003) and mitochondrial dysfunction causes the activation of caspase-9 and caspase-3.

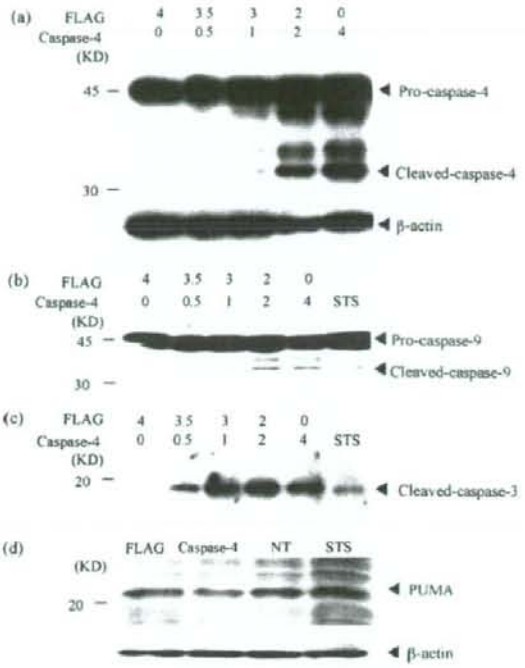

Fig. 2. Overexpression of caspase-4 increases the cleavage of caspase-3 and caspase-9. (a–c) COS-7 cells were transfected with the mixture of expression vectors for caspase-4-FLAG and FLAG as shown in this figure (0, 0.5, 1, 2 or 4 μg of caspase-4-FLAG expression vector were mixed with FLAG expression vector and total volume of each mixtures of the expression vectors was 4 μg). Twenty-four hours after transfection, equal amounts of cell lysates were analyzed by Western blotting using anti-caspase-4 (a), anti-caspase-9 (b) or anti-caspase-3 (c) antibody. As a positive control of cleaved caspase-9 or caspase-3, the lysates of 0.1 μM staurosporin (STS) -treated COS-7 cells were used. (d) Lysates of COS-7 cells transfected with 2 μg of expression vector for caspase-4-FLAG or FLAG were analyzed by Western blotting using anti-PUMA antibody. Overexpression of caspase-4 failed in the induction of PUMA, while STS treatment increased the expression level of PUMA in comparison with no treated COS-7 cells (NT) used as a negative control.

Thus, we examined the possibility that cleavage of caspase-9 and caspase-3 induced by the overexpression of caspase-4 is attributable to the mitochondrial dysfunction *via* activation of PUMA, but caspase-4 did not induce PUMA (Fig. 2d). These findings suggest that activation of caspase-3 and caspase-9 does not depend on the activation of PUMA, which causes the mitochondrial dysfunction. Next, we investigated whether caspase-4 provokes the effluent of cytochrome-*c* from mitochondria to cytosol using immunocytochemistry and Western blotting of subcellular fractionation. Either caspase-4-GFP or GFP, as a control, was overexpressed in COS-7 cells. The punctate distribution pattern of cytochrome-*c* observed in the cytoplasm of either caspase-4-GFP or GFP expressing COS-7 cells was similar to that of the no treatment cells (Fig. 3a). On the other hand, STS-treated cells showed a diffused distribution of cytochrome-*c* in cytoplasm (Fig. 3a). These results suggest that caspase-4 does not cause the release of cytochrome-*c*. To confirm this, we collected the cytosolic

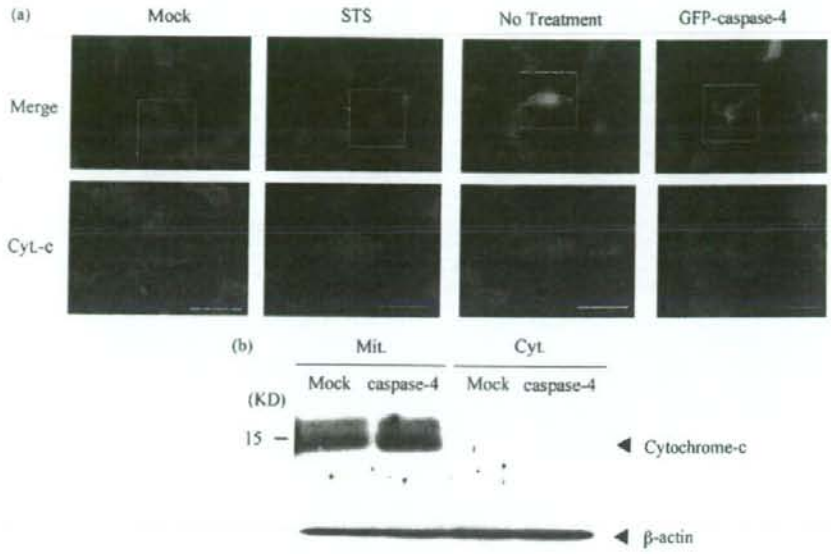

Fig. 3. Overexpression of caspase-4 does not have effects on the efflux of cytochrome-*c* from mitochondria to cytosol. (a) COS-7 cells were transfected with expression vector for caspase-4-GFP or GFP vector. 24 h after transfection, the cell were fixed and immunostained with anti-cytochrome-*c* antibody (red). Nuclei were visualized by DAPI as blue color. Green signal indicates GFP or caspase-4-GFP expressing cells. Lower panels show enlarged pictures of inserted boxes in each merged figures. Scale bar indicates 20 μm. (b) The cytosolic fraction and mitchondrial fraction were collected from the FLAG or caspase-4-FLAG expressing COS-7 cells or 0.1 μM staurosporin (STS) -treated or no treated COS-7 cells. Equal amounts of cell lysates were analyzed by Western blotting using anti-cytochrome-*c* (upper panel: the bands around 15 kDa indicate cytochrome-*c*) or anti- β-actin (lower panel) antibody.

fraction and mitchondrial fraction from the cells expressing caspase-4-FLAG or FLAG. Cytochrome-*c* could not be detected from the cytosol fraction of these cells (Fig. 3b). These data, with the previously described data, suggest that caspase-4 could activate caspase-9 and caspase-3 independently of the mitchondria-cytchrome-c pathway.

4. Discussion

Since caspase-12 has been shown to be involved in signaling pathways specific to ER stress-induced apoptosis (Nakagawa et al., 2000), caspase-12 has been believed to be involved in the pathogenesis of AD. However, since mature caspase-12 protein is not produced in humans (Fischer et al., 2002), caspase-12 does not function in ER stress-induced apoptosis such as AD, and some other caspases may play a key role in humans. Recently, we have found that caspase-4 can function as an ER stress-induced caspase in humans and may be involved in the pathogenesis of AD (Hitomi et al., 2004). The present study revealed that the familial AD-linked mutation (PS1ΔE9) enhances the cleavage of caspase-4 (Fig. 1) suggesting that caspase-4 plays a key role in the pathogenesis of AD.

Caspase-12-deficient mice show a reduced susceptibility to Aβ toxicity (Nakagawa et al., 2000). In humans, in which caspase-12 protein is not produced, caspase-4 functions similarly to mouse caspase-12 and is cleaved specifically by ER stress and Aβ treatment (Hitomi et al., 2004). Cell death induced by Aβ treatment is also partially inhibited by RNAi to caspase-4 (Hitomi et al., 2004). Thus, it is probable that in the human brain caspase-4 is involved in Aβ-induced cell death. From the aspect of Aβ, it could be concluded that activation of caspase-4 by ER stress and familial AD-linked mutations elevate the vulnerability of neurons to apoptosis, and is involved in the pathogenesis of AD.

Downstream events from caspase-4 are not fully understood. The present study has revealed that overexpression of caspase-4 results in the cleavage of caspase-3 and caspase-9 without the release of cytochrome-*c* from the mitochondria (Figs. 2 and 3). These findings indicate that caspase-4 functions using similar signaling pathways to caspase-12, which has been reported to activate downstream caspase-9 independently of cytochrome-*c* release (Morishima et al., 2002). But a clear mechanism of cleavage of caspase-3 and caspase-9 by ER stress is still obscure. PUMA, one of the BH3-only proteins, is induced *via* the p53 cascade under long term ER stress (Reimertz et al., 2003; Li et al., 2006). Induction of PUMA causes the dysfunction of mitochondria and the efflux of cytochrome-*c* from mitochondria to the cytosol, resulting in cell death through the activation of caspase-3 (Li et al., 2006). Accordingly, activation of caspase-3 and caspase-9 by the ER stress-induced cleavage of caspase-4 might be attributable to PUMA. However, in the present study, the overexpression of caspase-4 failed to induce the expression of PUMA, suggesting a lesser involvement of PUMA in the activation of caspase-3 and caspase-9 *via* caspase-4 (Fig. 2d). A faint relationship between mitochondrial function and capase-4 was also demonstrated by our previous study (Hitomi et al., 2004). Cleavage of caspase-4 is not affected by the overexpression of

Bcl-2, which prevents signal transduction on the mitochondria. In addition, the overexpression of caspase-4 failed to induce the efflux of cytochrome-*c* from mitochondria to cytosol (Fig. 3). Thus, caspase-4 could directly cleave caspase-3 and caspase-9 and induce cell death without involvement of mitochondrial apoptotic machinery.

In addition to AD, we have established that neuronal death caused by ischemia is also attributable to ER stress (Bando et al., 2003). Recently, the involvement of ER stress in neuronal death in Huntington's disease (Kouroku et al., 2002), Parkinson's disease (Ryu et al., 2002) and amyotrophic lateral sclerosis (Atkin et al., 2006) has been reported. Based upon these findings, it is likely that the activation of caspase-4 mediates neuronal cell death, not only in the AD, but also other neurodegenerative disorders. Accordingly, caspase-4 could be a potential target for the development of treatments for neurodegenerative diseases. For this purpose, it is important to screen the proteins interacting with pro-caspase-4.

Acknowledgements

This work was supported by grants from the Osaka Medical Research Foundation For Incurable Diseases. We are grateful Ms. Arakawa, Ms. Moriya and Ms. Ohashi for preparing the experiments.

References

Atkin, J.D., Farg, M.A., Turner, B.J., Tomas, D., Lysaght, J.A., Nunan, J., Rembach, A., Nagley, P., Beart, P.M., Cheema, S.S., Horne, M.K., 2006. Induction of the unfolded protein response in familial amyotrophic lateral sclerosis and association of protein-disulfide isomerase with superoxide dismutase 1. J. Biol. Chem. 281, 30152–30165.

Bando, Y., Katayama, T., Kasai, K., Taniguchi, M., Tamatani, M., Tohyama, M., 2003. GRP94 (94 kDa glucose-regulated protein) suppresses ischemic neuronal cell death against ischemia/reperfusion injury. Eur. J. Neurosci. 18, 829–840.

Fischer, H., Koenig, U., Eckhart, L., Tschachler, E., 2002. Human caspase 12 has acquired deleterious mutations. Biochem. Biophys. Res. Commun. 293, 722–726.

Hitomi, J., Katayama, T., Eguchi, Y., Kudo, T., Taniguchi, M., Koyama, Y., Manabe, T., Yamagishi, S., Bando, Y., Imaizumi, K., Tsujimoto, Y., Tohyama, M., 2004. Involvement of caspase-4 in endoplasmic reticulum stress-induced apoptosis and Abeta-induced cell death. J. Cell Biol. 165, 347–356.

Katayama, T., Imaizumi, K., Sato, N., Miyoshi, K., Kudo, T., Hitomi, J., Morihara, T., Yoneda, T., Gomi, F., Mori, Y., Nakano, Y., Takeda, J., Tsuda, T., Itoyama, Y., Murayama, O., Takashima, A., St. George-Hyslop, P., Takeda, M., Tohyama, M., 1999. Presenilin-1 mutations downregulate the signalling pathway of the unfolded-protein response. Nat. Cell Biol. 1, 479–485.

Kouroku, Y., Fujita, E., Jimbo, A., Kikuchi, T., Yamagata, T., Momoi, M.Y., Kominami, E., Kuida, K., Sakamaki, K., Yonehara, S., Momoi, T., 2002. Polyglutamine aggregates stimulate ER stress signals and caspase-12 activation. Hum. Mol. Genet. 11, 1505–1515.

Li, J., Lee, B., Lee, A.S., 2006. Endoplasmic reticulum stress-induced apoptosis: multiple pathways and activation of p53-up-regulated modulator of apoptosis (PUMA) and NOXA by p53. J. Biol. Chem. 281, 7260–7270.

Morishima, N., Nakanishi, K., Takenouchi, H., Shibata, T., Yasuhiko, Y., 2002. An endoplasmic reticulum stress-specific caspase cascade in apoptosis. Cytochrome c-independent activation of caspase-9 by caspase-12. J. Biol. Chem. 277, 34287–34294.

Nakagawa, T., Zhu, H., Morishima, N., Li, E., Xu, J., Yankner, B.A., Yuan, J., 2000. Caspase-12mediates endoplasmic-reticulum-specific apoptosis and cytotoxicity by amyloid-beta. Nature 403, 98–103.

Rao, R.V., Hermel, E., Castro-Obregon, S., del Rio, G., Ellerby, L.M., Ellerby, H.M., Bredesen, D.E., 2001. Coupling endoplasmic reticulum stress to the cell death program. Mechanism of caspase activation. J. Biol. Chem. 276, 33869–33874.

Reimertz, C., Kogel, D., Rami, A., Chittenden, T., Prehn, J.H., 2003. Gene expression during ER stress-induced apoptosis in neurons: induction of the BH3-only protein Bbc3/PUMA and activation of the mitochondrial apoptosis pathway. J. Biol. Chem. 162, 587–597.

Ryu, E.J., Harding, H.P., Angelastro, J.M., Vitolo, O.V., Ron, D., Greene, L.A., 2002. Endoplasmic reticulum stress and the unfolded protein response in cellular models of Parkinson's disease. J. Neurosci. 22, 10690–10698.

Sherrington, R., Rogaev, E.I., Liang, Y., Rogaeva, E.A., Levesque, G., Ikeda, M., Chi, H., Lin, C., Li, G., Holman, K., Tsuda, T., Mar, L., Foncin, J.F., Bruni, A.C., Montesi, M.P., Sorbi, S., Rainero, I., Pinessi, L., Nee, L., Chumakov, I., Pollen, D., Brookes, A., Sanseau, P., Polinsky, R.J., Wasco, W., Da Silva, H.A.R., Haines, J.L., Pericak-Vance, M.A., Tanzi, R.E., Roses, A.D., Fraser, P.E., Rommens, J.M., St. George-Hyslop, P., 1995. Cloning of a gene bearing missense mutations in early-onset familial Alzheimer's disease. Nature 375, 754–760.

Yankner, B.A., Dawes, L.R., Fisher, S., Villa-Komaroff, L., Oster-Granite, M.L., Neve, R.L., 1989. Neurotoxicity of a fragment of the amyloid precursor associated with Alzheimer's disease. Science 245, 417–420.

Yoneda, T., Imaizumi, K., Oono, K., Yui, D., Gomi, F., Katayama, T., Tohyama, M., 2001. Activation of caspase-12, an endoplastic reticulum (ER) resident caspase, through tumor necrosis factor receptor-associated factor 2-dependent mechanism in response to the ER stress. J. Biol. Chem. 276, 13935–13940.